DESIGN AND MIXING PERFORMANCE OF PASSIVE MICROMIXERS: A CRITICAL REVIEW

Afzal Husain[1*], Asharul Islam Khan[1], Wasim Raza[2], Nabeel Al-Rawahi[1], Nasser Al-Azri[1], and Abdus Samad[2]
[1]Mechanical and Industrial Engineering Department, Sultan Qaboos University, Muscat, Oman
[2]Department of Ocean Engineering, Indian Institute of Technology Madras, Tamil Nadu, India.

ABSTRACT: This study extracts and reports notable findings on passive micromixers by conducting an exhaustive review of designs, their features, and mixing performance. The study has covered the relevant articles on passive micromixers published from 2010 to 2020. The analysis of filtered and selected articles sums up passive micromixers into four categories: designed inlets, designed mixing-channel, lamination-based, and flow obstacles-based. The prominent mixing channel categories identified in the study are split-and-recombine (SAR), convergent-divergent (C-D), and mixed (SAR, C-D, and others). Moreover, differences in mixing channel designs, number of inlets, and evaluation methods have been used in comparing the mixing performance of passive micromixers. The SAR and the obstacles-based micromixers were found to outperform the others. The designs covered in the present review show significant improvements in the mixing index. However, these studies were conducted in an isolated environment, and most of the time, their fabrication and device integration issues were ignored. The assortment and critical analysis of micromixers based on their design features and flow parameters will be helpful to researchers interested in designing new passive micromixers for microfluidic applications.

Keywords: Microfluidics, Passive micromixers; Mixing index; Split-and-recombine; Convergent-divergent; Lamination; Off-set inlets.

تصميم وفعالية الأداء للخلاطات الدقيقة غير النشطة: مراجعة نقدية

أفضال حسين وأشار الإسلام خان ووسيم رضا ونبيل الرواحي وناصر العزري وعبد الصمد

الملخص: تقوم هذه الدراسة على استخلاص ونشر أهم البيانات عن الخلاطات الدقيقة السلبية بعد مراجعة شاملة عن تصاميم ومميزات وأداء هذه الخلاطات حيث استهدفت هذه الدراسة المنشور عن الخلاطات الدقيقة السلبية بين العامين 2010 و2020م. وبعد فرز هذه الدراسات وتحليلها نجد أن الخلاطات الدقيقة السلبية يمكن تقسيمها بناء على أربعة محاور: تصميم المداخل وتصميم قناة الخلط وخاصية التغليف وعوائق الدفق. وخلصت هذه الدراسة إلى أن أبرز الفئات المبنية على قناة الخلط هي: الفصل وإعادة الجمع، والمتقاربة-المتباعدة القطر والمتعددة الأنواع. بالإضافة إلى ذلك فإن مقارنة أداء الخلط في هذه الدراسة تم بناؤها على الاختلاف في تصميم قنوات الخلط وعدد المداخل وطرق التقييم. تبين كذلك أن خلاطا الفصل وإعادة الجمع وتلك المبنية على عوائق الدفق تتفوق في أدائها عن الخلاطات الدقيقة السلبية الأخرى. كما أن التصاميم التي شملتها هذه المراجعة قد أثبتت تطورات هامة في مؤشرات الخلط. إلا أن ما يجدر ذكره أن هذه الدراسات قد أجريت في بيئات معزولة كما يغلب عليها إهمال جانب طبيعة تصنيع هذه الخلاطات والقضايا المتعلقة بتكامليتها مع الأجهزة الأخرى. إن تصنيف وتحليل الخلاطات الدقيقة بناء على مزايا تصميمها ومعاملات الدفق فيها سيساعد الباحثين المهتمين بتصميم خلاطات دقيقة جديدة في تطبيقات الموائع الدقيقة.

الكلمات المفتاحية: الموائع الدقيقة؛ الخلاطات الدقيقة السلبية؛ مؤشر الخلط؛ الفصل وإعادة الجمع؛ التقارب والتباعد؛ التغليف؛ المداخل المزاحة.

Corresponding author's e-mail: afzal19@squ.edu.om

DOI:10.53540/tjer.vol19iss2pp106-128

1. INTRODUCTION

A passive micromixer is an important component of lab-on-chip devices. They are one of the most frequently used add-ons in microfluidics for rapid mixing. Micromixers are getting extensive attention in numerous fields of science and engineering disciplines such as biochemical analysis, drug discovery, sensing, microelectromechanical systems (MEMS), micro total analysis systems (μ-TAS), bio-diagnostics, Lab-on-a-Chip (Johnson and Locascio, 2002), and chemical processing. It can be used standalone as well as an integrated mixing unit in microfluidic systems. Micromixers are used to mix two or more fluids rapidly within a short channel length and short time. The advantages associated with the micro-dimension of channels, such as reduced sample volume and reagent requirement along with the lesser amount of waste-product produced, lead to low operating cost, high surface area to volume ratio providing better heat dissipation, faster analysis results, portability, and high-throughput through parallelization. These advantages have enhanced their prospects of usage in a wide range of applications such as DNA purification (Kastania *et al.*, 2016), protein folding (Jang *et al.*, 2019), enzyme catalysis (Zhang *et al.*, 2021), nanoparticle synthesis (Westerhausen *et al.*, 2016), and water quality monitoring. An exhaustive review of the applications of micromixers can be found elsewhere (Jaywant and Arif, 2019; Jeong *et al.*, 2010; Lee and Fu, 2018).

The micromixer design, passive structures, and the flow Reynolds number (*Re*) significantly affect the mixing performance and need further research to meet the contemporary developments in the microsystems. The Reynolds number indicates the degree of dominance of inertial force over viscous force. Turbulent flow, characterized by a high Reynolds number (Re > 2300), has greater inertial force causing flow instabilities in the form of vortices and eddies, which can promote mixing in the channel. However, the flow Reynolds number in a micromixer (Re < 100) is much lower than the limiting Reynolds number for a turbulent flow (Re > 2300). Hence, the adequate mixing of two fluids is difficult to achieve in the absence of flow instability under laminar flow conditions inside the micromixers (Re<<100) as compared to the turbulent flow (Bhopte *et al.*, 2010). Mixing by diffusion is a slow process, which has little relevance to most fluid mixing applications, where fast mixing is a prerequisite. Thus, microfluidic mixing is a challenging problem for low diffusivity fluids under laminar flow conditions and hence requires design improvements to enhance mixing.

The micromixers are of the types: active, passive, and hybrid. In addition, each of them has many sub-classifications based on the channel designs and mixing mechanism. The mixing in active micromixers needs external forces like the electric field, acoustic field, magnetic field, and thermal field to disturb the flow. However, mixing in passive micromixers occurs due to molecular diffusion and chaotic advection strengthened through channel structural modifications. Passive micromixers are low-cost, reliable, robust, efficient, and easy to use. Passive micromixers have been used in mixing both miscible and immiscible fluids. The hybrid micromixers use important characteristics of both active and passive micromixers to enhance the mixing capabilities (Bazaz *et al.*, 2018). The passive micromixers are of Y- and T-shape depending on the inlet design. They also differ in terms of mixing-channel configurations, such as obstacles in the main channel or attached to the walls, and designed mixing-channel geometry profiles (e.g., zigzag, Split-and-Recombine (SAR), and a teardrop). There is a proportional relationship between flow path length and mixing performance based on the localized mixing and global mixing principles (Su *et al.*, 2019).

The mixing efficiency/performance of the passive micromixer is largely dependent on the geometric layouts and Reynolds number. Thus, there is a striking possibility to achieve different levels of mixing by tweaking and tuning the geometric parameters. For example, in the case of Imitate Cantor structure passive micromixers, reducing space between adjacent fractal obstacles in the mixing channel and increasing the mixing chamber's height improve the mixing performance (with optimum mixing performance at 600 µm height) (Wu and Chen, 2019a). In chaotic advection-type passive micromixers having dual opposing structures on microchannel walls, the alignment of structure strips affects the mixing performance (Chen *et al.*, 2015). The mixing performance is enhanced by interdigital inlets (Cook *et al.*, 2011). Additionally, the geometric-parameters tolerances associated with any fabrication process slightly influence the performance of the passive micromixers. Further, in a study, the authors calculated the cumulative distribution function for three cases to obtain the probability of having mixing efficiency lower than 95% for a Tesla micromixer (Stanciu, 2015). For instance, a small change (up to 5%) in geometric parameters with six and seven elements yields respective probabilities of 11.1% and 2.08% for getting mixing performance lower than 95% (Stanciu, 2015).

Although there has been a large array of improvements achieved in the last few years, intense research for more efficient passive micromixers for microfluidic systems is continued to date. Most of the research has focused on the design of new passive micromixers and the estimation of their mixing performance through experiments and numerical simulations. Furthermore, several studies have reviewed the literature on micromixers, such as a comparative review on passive micromixers (Raza *et al.*, 2020), a review on droplets based micromixers (Chen *et al.*, 2019a), a review on active and passive micromixers (Bayareh *et al.*, 2019), a short review on micromixers classification (Mukhopadhyay, 2018),

and a review on micromixers (Gaozhe *et al.*, 2017). These studies are mainly focused on passive micromixers, their types, and to some extent, fabrication techniques, with some emphasis on micromixers having both passive and active mixing features. There is a significant void in the literature to get a comprehensive spectrum of passive micromixers, their capabilities, applications, and feasibility of integration. Nevertheless, this review investigates the dominant microchannel structures adopted for mixing enhancement in the last decade. Additionally, it sets the base to propose favorable channel structures to be further explored in the future. The study conducts an extensive analysis of the published findings on passive micromixers from the year 2010 to 2020. There are six sections in the article. Section 1 briefly introduces the concept and challenges of passive micromixing, Section 2 illustrates the research method, Section 3 corresponds to the background study, Section 4 aggregates the literature from 2010 to 2020 and classifies passive micromixers, Section 5 presents the analysis and discussion, and the Section 6, the last section, summarizes the findings and discusses future research.

The study has followed a systematic literature review approach. Several protocols were set, including the databases to search for articles, inclusion and exclusion criteria for articles, and extraction of relevant information from the filtered articles. This approach helps in getting articles objectively rather than the exploration of databases randomly. The systematic literature review has become a common method of conducting a literature review in different fields of science and engineering. The online databases referred to for collecting the articles include Science Direct, Google Scholar, Springer, and IEEE Xplore. Articles published only in English and published in the years between 2010 and 2020 were considered.

2. BACKGROUND

The fluid flow in microchannels is mostly laminar when the channel is of small dimensions, and fluid velocity is low (Bayareh *et al.*, 2019). The efficiency and sensitivity of microfluidic devices are influenced by the passive structures in the micromixers and their designs (Gaozhe *et al.*, 2017). The micromixers found in the literature can be broadly categorized into four principles such as lamination-based, injection-based, droplets-based, and chaotic advection-based (Figure 1). The lamination-based micromixers can be further categorized into parallel and serial lamination-based passive micromixers. In addition, they are sub-classified into; channels with obstacles (or baffles), curved-channel, convergence-divergence, and unsymmetrical (Bayareh *et al.*, 2019). The lamination-based micromixers have a layered structure, and they achieve excellent mixing in a short time (milliseconds) (Gaozhe *et al.*, 2017). The micromixers based on injection have nozzles through which fluid passes in the form of many sub-streams into the mainstream. The droplet-based passive micromixers inject droplets for mixing (Yang *et al.*, 2018) into the main channel. The micromixers based on chaotic advection work on the principle of stretching, folding, and breaking of fluid interfaces for the laminar flow. Mixing in passive micromixers is mainly due to the phenomena of molecular diffusion and chaotic advection. The chaotic advection is favorable when the fluids have large size molecules and small diffusion coefficients. This study classifies passive micromixers based on inlet designs (designed inlets), mixing-channel layout/design, lamination-based, and obstacle-based (Figure 2).

2.1 Designed Inlets

The mixing performance of passive micromixers varies with the type of inlets. The designed inlets include (1) an angle between the two inlets (T-, Y-, and configuration with other angles), (2) swirl-induced inlet, and (3) numbers of the inlet (e.g. 2, 3, 4, and 5). The mixing performance of passive micromixers increases with the angle between inlets. The inlet angle has been varied from 60° to 300°; however, the commonly designed inlets are T- and Y-shape (Figure 3). Figure 3 shows the designed inlets and their arrangements at different angles.

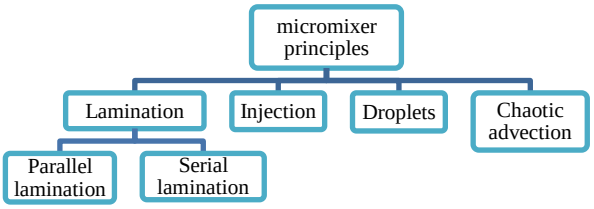

Figure 1. Working principles of passive micromixers.

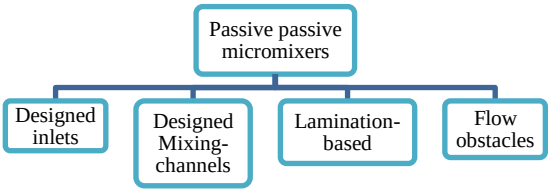

Figure 2. Classification of micromixers based on geometric features.

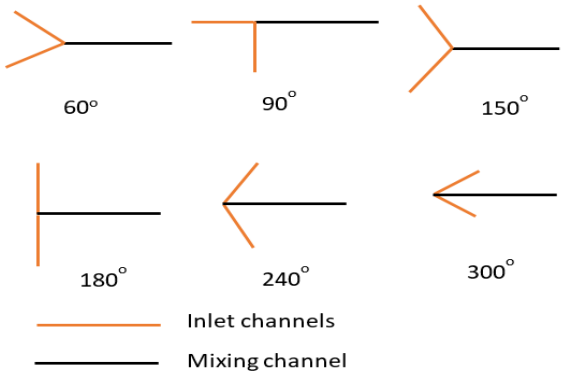

Figure 3. Micromixers based on inlet channels.

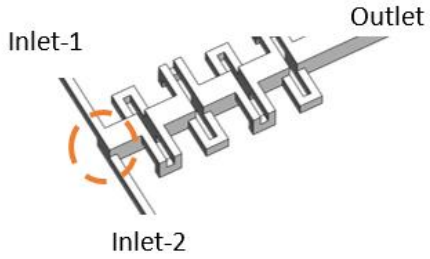

Figure 4. Micromixer with swirl inlets.

It was suggested that the optimal inlet mixing angles are 90°-180° for high mixing and low energy dissipation (Zhang *et al.*, 2016). The maximum and minimum mixing performances were obtained with an intersection of 300° between the inlets at *Re* values of 60 and 80 (Zadeh and Marahel, 2011), respectively. In addition to various configurations of the inlets, the swirl inlets (Figure 4) have shown a considerable impact on the mixing performance. For example, the T-shape micromixers with swirl inlets showed a mixing enhancement by a factor of more than two compared to a T-mixer at *Re* = 20–150. Additionally, a T-shaped micromixer with swirl inlets achieved a mixing index of 40 times that of the simple T-micromixer at *Re* = 100. In the three-dimensional serpentine micromixers, the impact of the antisymmetric inlets was significant at the early stage; mixing index enhancement of 2–10 times was observed at *Re* = 100 (Matsunaga and Nishino, 2014).

The swirl in the inlets improves the mixing performance at intermediate Re values (66 < *Re* < 180). The reverse orientation swirl (R-O-Swirl) inlets micromixers performed better than the same orientation swirl (S-O-Swirl) inlets micromixers. Dundi *et al.* (2019) found that the mixing performance of a micromixer with R-O-Swirl inlets increases 300% to 400% at 160 < *Re* < 180 and with S-O-Swirl inlets increases 30% to 70% at 266 < *Re* < 372, as compared to a T-shape passive micromixer without swirl. Although the simplest T- and Y-shape passive micromixers have two inlets, there are passive micromixers with more than two inlets. In Y-shape passive micromixers with three inlets, the pressure drop is uniform, and fluid flows with constant velocity, resulting in fast diffusion of fluids (Adam and Hashim, 2012). The four-inlet passive micromixers can have 50% less pressure drop and improved mixing performance of 300% to 500% as compared to the normal passive micromixers (Bhopte *et al.*, 2010). The swirl-induced two-inlets passive micromixers have higher numerical diffusion than the swirl-induced four-inlet passive micromixers at 120 < *Re* < 240 (Okuducu and Aral, 2019a).

In general, swirl inlets and reverse-oriented swirl inlets have shown significant improvement especially advection-driven mixing at higher Reynolds numbers. These inlet designs can be looked at for integrating with other 3D designs of the main channel to achieve higher mixing in a shorter length.

2.2 Mixing-channel layout/design-based

The channel layout plays an important role in enhancing the mixing performance. Passive micromixers with hydrophobic microchannels have better performance than hydrophilic microchannels. The spiral microchannels produce higher mixing performance as compared to straight microchannels (Zhang *et al.*, 2016). The prominent two-dimensional (2D) and three-dimensional (3D) microchannel layouts are spiral and wave (e.g., single spiral, double spiral, helical, sinusoidal, rectangular, square, and zigzag), SAR, and convergent-divergent (CD), and mixed (SAR, CD, and others).

2.2.1 Wave/Spiral shaped microchannel

This section dealt with the wave and spiral-shaped mixing-channel designs proposed in the last decades. Chen *et al.* (2016a) reported the shape optimization of a micromixer with six different channel layouts. The authors found that the square wave microchannel produced the highest mixing performance among the tested six layouts. The order of decreasing mixing performance was square wave > multi-wave > zigzag > T > mouth > loop micromixers (Chen *et al.*, 2016a). Scherr et al. (Scherr *et al.*, 2012) proposed a micromixer based on logarithmic spirals and measured the mixing performance at the Reynolds number varying between 1 and 70. They noticed a decline in mixing as the *Re* values increased from 1.0 to 15 with a transition at *Re* = 15 (mixing efficiency = 53%); however, mixing increased with a further increase in *Re* and reached 86% at *Re* = 67. The new design showed higher mixing as compared to the Archimedes spiral and Meandering-S mixers. Papadopoulos *et al.* (2014) investigated the effects of inlet velocity in a zigzag microchannel geometry with a T-inlet. It was reported that the number of zigzags affects the mixing at a fixed inlet velocity. A higher velocity requires a larger number of zigzags for efficient mixing. A total of 150 zigzag units were recommended to achieve efficient mixing performance (98%) at a velocity of 2 *mm/s* and at a diffusion coefficient of 10^{-10} m^2/s.

Wang *et al.* (2018) designed a modified S-shaped microchannel having asymmetric lateral wall structures and conducted numerical simulations for both the modified microchannel and simple S-shaped microchannel at *Re* values ranging from 0.1 to 100. They found that as *Re* values increase from 0.1 to 100, modified S-shaped microchannel exhibits high mixing performance than simple S-shaped. It is due to the formation of secondary flow and higher inertial effects. Rafeie *et al.* (2017) proposed a 3D fine-threaded lemniscate-shaped micromixer to overcome the limitations of other 3D micromixers. They reported a mixing performance of over 90% at Reynolds numbers ranging from 1.0 to 1000, both numerically and experimentally. They observed that the chaotic advection (due to Dean flow) and diffusive mixing (due

to grooves) are the main cause of high mixing.

Zhang *et al.* (2012) proposed a 3D-twisted compression–expansion microchannel for passive micromixers. They applied simulations to compare the new design with a T-shape having the same cross-sectional perimeters. The new design was reported to have higher mixing efficiency compared to T-mixer. Moreover, clamping angles at 90 degrees, 45−90 degrees, and 45 degrees have different efficiency outputs, with maximum efficiency reported at 45 degrees causing the least pressure drop. Yang *et al.* (2013) proposed a micromixer with overlapping dual spirals. The micromixer showed enhanced performance due to sustained Dean vortices. There are several studies on mixing-channel design with a helical structure and its variations. The helical structure can be single or double. Liu *et al.* (2015) studied 3D cross-linked double-helical microchannel for fast mixing at low-*Re* value. They compared the new channel with a helical and a straight channel of the same dimensions. The numerical Simulation revealed higher mixing of the 3D cross-linked double-helical microchannel with full mixing within three cycles at *Re* = 0.0015~600. The helical microchannel in 3D micromixers introduces chaotic advection, and the double helix has an agitation effect.

Viktorov and Nimafar (2013) analyzed numerical and experimentally mixing performance and pressure drop in two micromixers (chain one and chain 2) consisting of 3D SAR with a special arrangement of microstructures called 'chain mixer'. They found that the chain and teardrop micromixer, due to the SAR mechanism, have higher mixing performance (reached up to 98%) compared to a simple T-shape and O-shaped mixer for Reynolds numbers ranging from 0.083 to 4.166. Furthermore, chain mixers showed lower pressure drop as compared to teardrop mixers. Al-Halhouli *et al.* (2015) designed ILSC and *Ω* channels to enhance mixing efficiency by introducing the Dean Vortices and molecular diffusion. They compared the performance of new designs with a spiral design using numerical Simulation and experiment. The ILSC and *Ω* configurations have complete mixing when the Reynolds number lies between 0.01 and 50, and on the other hand, the complete mixing in the semicircle shapes arranged in a spiral occurred at *Re* > 50.

Afzal and Kim (2015b) numerically carried out multi-objective Optimization of the sigma micromixer using a multi-objective genetic algorithm. The author observed that the geometric parameters could be effectively fixed to maximize the mixer performance. The square-wave channel exhibited significant improvement over other wavy channels and is simpler in fabrication. It is found that in spiral micromixers, repetitive alteration of the flow direction has improved the mixing in a wide range of Reynolds numbers due to changes in Dean vortices' rotational direction. Furthermore, a design with a smaller radius of curvature is better for mixing.

2.2.2 SAR-based microchannel

The microchannel based on the SAR principle has higher mixing performance as compared to non–SAR (Ansari and Kim, 2010). The SAR-based microchannel can be with a chamber and without a chamber. The chambered SAR design has several variations as circular, elliptical, and rhombus. The splits in the chambered SAR can be two or more.

Moreover, Gidde *et al.* (2019b) numerically investigated the impact of balanced and unbalanced splits on the mixing performance and pressure drop in the circular split and recombine (CSAR) and elliptical split-and–recombine (ESAR) (Cortes-Quiroz *et al.*) micromixers at Reynolds numbers ranging from 0.1 to 75. They observed that at $0.1 \leq Re \leq 5$, mixing is due to diffusion, while for $Re > 5$, mixing is caused by the secondary flow, separation vortices, and SAR effect. The ESAR micromixer (with balanced and unbalanced split) has higher mixing performance and less pressure drop than the CSAR micromixer over the entire range of *Re* and showed good mixing performance at Reynolds numbers ranging from 20 to 75.

Xia *et al.* (2011) investigated experimentally and numerically mixing performance in a planar asymmetric split-and-recombine micromixer with a fan-shaped cavity at *Re* = 1–80. They observed higher mixing due to the combination of expansion vortices (caused by the converging-diverging structure of the fan-shaped cavity) and Dean Vortices, along with unbalanced inertial collisions. The proposed micromixer having a fan-shaped cavity of width equal to three times the width of the major sub-channel, achieved a mixing index of around 75% at $Re \geq 60$.

Hossain and Kim (2014) designed a passive micromixer with unbalanced three-split rhombic sub-channels and evaluated performance against a two-split micromixer at several Reynolds numbers ranging from 0.1 to 120. They observed that the mixing performance of the three-split rhombic microchannel is 1.49, 1.67, 1.56, and 1.44 times higher than the corresponding two splits at *Re* = 30, 40, 50, and 60, respectively. Further, Hossain and Kim (2015) investigated the mixing performance of a 3D serpentine split-and-recombine microchannel consisting of a series of "OH"-shaped segments in a Reynolds number range of 0.1–120. They observed that continuous split-and-recombine of the fluid streams due to the O- and H-structures generates chaotic advection and thereby improves the mixing. The inclusion of SAR design with the serpentine structure improved the mixing performance compared to a previously proposed 3D serpentine design in a Reynolds number range of 0.1–70.

Gidde *et al.* (2019a) numerically investigated the flow features, mixing performance, and pressure drop in a proposed eye-shaped split and collision (ES-SAC) passive micromixer for *Re* ranging from 0.1 to 45. They reported that mixing performance is enhanced due to the unbalanced collision of the two fluid streams in the sub-channels of unequal widths. Among three different ratios of the sub-channel width, i.e., 1, 1.4,

and 2, the least mixing was observed for the width ratio of 1, while the highest mixing was observed for the width ratio of 2. Furthermore, the pressure drop in the micromixer with a sub-channel width ratio of 2 was the least among the three different width ratios. Nimafar *et al.* (2012) proposed a microchannel of an H-shape in which the fluid split and repeatedly recombined to maximize the diffusive mixing. The experimental Investigation demonstrated that H-micromixer was more efficient than the other two tested devices, i.e., T- and O-micromixer, in the Reynolds number range of 0.08–4.16. The new H-micromixer indicated a mixing performance of 98% at $Re = 0.083$.

Viktorov *et al.* (2015) proposed two modified designs of chain mixers, i.e., the Y-Y and the H-C microchannel based on the SAR principle, and investigated mixing and flow numerically and experimentally for Reynolds numbers ranging from 1 to 100. The mixing efficiency of these two passive micromixers showed flat characteristics with a value higher than 90% over the entire range of the Reynolds number investigated, while the mixing efficiency of the teardrop mixer showed a decrease in the mid-range of the Reynolds number. Moreover, the pressure drop was also less in the newly proposed designs as compared to the teardrop micromixer.

Ansari *et al.* (2010) evaluated the mixing performance of a SAR micromixer having sub-channels of unequal widths using numerical simulations and experiments at different Reynolds numbers between 10 and 80. The sub-channels of unequal widths caused unequal mass flux splitting and unbalanced collision on the recombination of mixing species. The combined effect of SAR, unbalanced collisions of the fluid streams, and Dean Vortices in the curved channels caused mixing enhancements. When the major sub-channel was twice as wide as the minor sub-channel, maximum mixing performance was achieved at a Re value greater than 40.

Ruijin *et al.* (2017) proposed a passive micromixer that generates continuous lamination layers using Baker transformation for mixing enhancement. They investigated the mixing performance numerically for Reynolds numbers ranging from 0.01 to 10 and compared its performance against other splitting-merging micromixers such as Helical-mixer and Smale-mixer. They found that the Baker mixer achieved higher mixer efficiency due to a better stratification effect than those in the Helical-mixer and Smale-mixer at low Reynolds numbers. However, due to the convection–dominant mixing at the higher Reynolds numbers, the Baker mixer showed lower mixing compared to the other two mixers. Furthermore, due to the presence of contracting channels in the Baker mixer, the pressure drop through it was higher than that in the other two mixers.

Pennella *et al.* (2012) reported planar SAR micromixers with variable curvature, i.e., clothoid-shaped mixing units. They investigated the mixing performance numerically and experimentally for a Reynolds number range of 1 to 110. Due to the secondary flows in the repetitive mixing units and recirculation effects at the junctions of the unit, the proposed mixer achieved a mixing efficiency of 80% for the Reynolds number greater than 70. Yang *et al.* (2015) proposed a passive micromixer with 3D Tesla structures and investigated the mixing performance experimentally and numerically for Reynolds numbers ranging from 0.1 to 100. The proposed micromixer showed a maximum mixing efficiency of 94% and a pressure drop of less than 1054 Pa at $Re = 100$.

Le *et al.* (2014) designed a microchannel that utilizes the impact of stretching-folding in both vertical and horizontal directions through vortices and transverse flow to enhance the performance even for low *Re* values. They evaluated the mixing performance numerically and reported high efficiency (more than 80%) for Reynolds numbers ranging from 0.5 to 60. The new design indicated 220-240% higher mixing efficiency than a rhombic mixer with branch channels and pure rhombic at a low-*Re* value. Ta *et al.* (2015) proposed a trapezoidal channel arranged in a zigzag pattern (TZM) for mixing based on the SAR principle at low *Re*. The numerical simulation results indicated a mixing efficiency of more than 81% for *Re* values in the range of 0.1 to 80. For $Re \leq 0.9$ and $Re \geq 20$, the mixing efficiency was more than 90%. Additionally, the mixing efficiency of the proposed design was 4.07 and 5.58 times as compared to three-split rhombic and T-shape micromixers, respectively, at $Re = 20$. The high mixing was due to the transverse flows and distortion of fluid streams.

Sheu *et al.* (2012) performed numerical simulations and experiments for the mixing analysis of the proposed micromixers consisting of several staggered three-quarter ring-shaped channels and a semi-circular channel. They found that the staggered curved-channel mixer with a tapered channel achieved 20% higher mixing efficiency with 50% more pressure drop compared to the staggered curved-channel mixer with or without sudden-contracted channels. The Dean vortices formed in the curved channels due to uneven split-and-recombine structures and impingement effects enhanced the mixing in the channel. Tran-Minh *et al.* (2014) proposed a microchannel based on the SAR principle with ellipse-like micro-pillars and determined the performance using numerical simulations. The proposed design attained a mixing efficiency of 80% for *Re* values in the range of 1 to 80.

Kefala *et al.* (2014) proposed a SAR mixer design with multiple labyrinthine spirals and conducted numerical simulations to compare its performance with the zigzag, spiral, and linear designs. They observed that the labyrinthine microchannel has higher mixing performance (63%) compared to the spiral (36.5%) and zigzag (35.5%) designs at $Re = 0.5$. The microchannel with spiral, zigzag, and labyrinthine designs showed higher mixing by 8%, 11%, and 92%, respectively, compared to the T-shape mixer.

Chen *et al.* (2018) modified a previously existing

F-shaped mixer to propose three designs, namely E-shape, stacking E-shape micromixer (SESM), and folding E-shape micromixer (FESM). They evaluated their performance experimentally for *Re* values in the range of 0.5 to 100. The new designs work on the chaotic advection and SAR mechanism. The mixing efficiency of the F-mixer and E-mixer started to decrease after reaching a maximum value of 92% and 94%, respectively, at *Re* = 80. However, the mixing efficiency of FESM and SESM remained close to 100%. For $25 \leq Re \leq 80$, all three modified designs performed better than the F-shaped mixer. At $Re > 80$, the mixing performances of two-layer mixers were better than single-layer mixers.

The SAR, in general, increases mixing performance due to bifurcation and collision. However, its effects are prominent in the advection regime. The unbalanced SAR shows improved performance over balanced SAR designs. Further, the square and elliptical-shaped mixing channels exhibited higher mixing performance than circular channels. The contraction and expansion of Dean vortices and distortion of flow streams increase fluid chaos resulting in enhanced mixing.

2.2.3 Convergent-divergent microchannels

The passive micromixers with microchannel based on the Convergent-Divergent (C-D) principles have mixed first by the convergence of fluids and then by divergence repeatedly. The convergence of the fluid streams reduces the diffusion path length, which enhances the mixing. Furthermore, the fluid layers get stretched on entering the divergent section, which increases the surface area across which diffusion occurs. In addition, due to the sudden expansion of the flow area at high Reynolds numbers, expansion vortices are generated that contribute to mixing. Gidde *et al.* (2018) compared the mixing performance of passive planar micromixers having circular- and square-shaped mixing chambers numerically, at Reynolds numbers ranging from 0.1−75. At *Re* = 0.1, 1, and 5, both designs exhibited similar mixing performance; however, the micromixer with square chambers showed higher mixing performance (99% when *Re* < 1) compared to the circular chambered micromixer. Moreover, both designs with a constriction width of 200 μm attained a mixing index over 95% in a Reynolds number range of 15–75.

Afzal and Kim (2015a) designed a C-D channel with sinusoidal channel walls. The C-D channel with sinusoidal walls was found to have 19% higher mixing efficiency as compared to straight, square-wave, zigzag, and sinusoidal microchannels with uniform cross-sections for a fixed mixing length. Further, the new design achieved 92% mixing performance (independent of *Re* in a range of Reynolds number, $0.25 \leq Re \leq 4$) when sinusoidal walls have two periods.

The design parameters, i.e., the aspect ratio of the cross-section, the ratio of amplitude to wavelength, and the Re values, affect the mixing performance of passive micromixers based on the C-D principle. Parsa *et al.* (2014) proposed a sinusoidal microchannel with C-D and evaluated the mixing performance by applying numerical simulations and experiments. They observed that the increase in the aspect ratio of the microchannel cross-section improves the mixing performance and reduces the pressure drop due to Dean Vortices formation for *Re*-value ranging from 0.2 to 50. Khan and Tandon (2017) modified a C-D channel as a wing-shaped and serpentine square wave and evaluated mixing performance via numerical simulations for *Re* values from 0.01 to 100. They found that a wing-shaped microchannel produced a mixing performance of 87% with a pressure drop of 72 *k Pa* at *Re* = 60. Additionally, a wing size of 100-μm gives better mixing efficiency than the 75-μm wings.

Rampalli *et al.* (2020) modified serpentine square wave micromixers by replacing square wave with convergent-divergent portion and evaluated the mixing efficiency for low Reynolds numbers (*Re* < 100). They found that for *Re*-value less than ten, diffusion mechanism-controlled mixing in square wave convergent-divergent (SQW-CD) mixer, stretching and folding due to C-D caused mixing when *Re* value was greater than 10. The SQW-CD mixer performed better than the conventional square wave mixer when *Re*-value was greater than 10.

Hong *et al.* (2019) designed a gourd-shaped (contract and expand) microchannel and performed a numerical simulation to evaluate the mixing performance (*Re* values from 1 to 100). The enhancement of mixing was due to vortex generation in the proposed design, and it achieved a mixing efficiency of 83% with a pressure drop of 4860 *Pa* at *Re* = 100.

The aspect ratio, amplitude, and pitch of the converging-diverging units play a significant role in mixing enhancement along with the contraction and expansion of the fluid streams. Further, a spiral channel with sinusoidal wave-shaped mixing units, which inherently consists of convergent and divergent portions, shows better mixing due to the synergetic effects of Dean vortices, folding, and stretching of fluid interfaces.

2.2.4 Hybrid design based on combined structures of SAR, C-D, and others

There is a number of passive micromixers based on SAR, C-D, and other principles combined to achieve higher mixing at different values of *Re*.

Afzal and Kim (2012) introduced a hybrid design using principles of both SAR and C-D. The new design has convergent-divergent channel walls with sinusoidal variations, besides splitting the main channels into two and recombining. They measured the impact of the Reynolds number (between 10 and 70), sinusoidal wall amplitude, and channel aspect ratio on the mixing efficiency. They observed a symmetric double vortex pair at the throat of the convergent-divergent channel and secondary motions in the sub-channels, which enhanced the mixing performance.

Numerical simulation results revealed that the new design has a higher efficiency compared to the T-mixer and unbalanced split and collision micromixer.

Gidde and Pawar (2020) studied numerical flow features and mixing performance of rectangular baffle-based triple split-and-recombine (RB-TSAR) and elliptical baffle-based triple split-and-recombine (EBTSAR) micromixers. Baffles of rectangular and elliptical shapes were placed in diffuser-shaped mixing chambers to generate flow in the transverse direction through the SAR mechanism. Baffles increase the contact area between the layers of mixing species by deflection and folding, thereby contributing to the mixing. The micromixer with elliptical baffles showed better mixing and less pressure drop compared to the micromixer with rectangular baffles due to strengthened secondary flow, separation vortices, and less flow resistance caused by the curved shape. Furthermore, the increase in the divergence angle of the diffuser caused mixing to improve and a reduction in pressure drop.

Fan and Hassan (2010) studied experimentally, and numerically a scaled-up micromixer having units called cross and omega at $1 \leq Re \leq 50$. In addition to the Dean vortices at high Reynolds numbers, split-and-recombine in cross units and focusing/diverging in the omega units were the main mixing mechanisms. The proposed design with five cells achieved a mixing efficiency of 70% at $Re = 50$, which indicates that this design can be used at high flow rates. Xie *et al.* (2010) introduced a new design of micromixers with eight semicircles in the microchannel and measured mixing performance both numerically and experimentally for *Re* values in the range of 0.08 to 40. They observed higher mixing performance (i.e., 90%, for $Re < 0.1$ and $Re > 10$) compared to a simple T-shape mixer.

Moghimi and Jalali (2020) proposed a micromixer in which mixing occurred through multi-lamination and flow-resistance reduction caused due to combined usage of injection and recombination in a zigzag layout. Experimental and numerical results indicated that the proposed mixer attained a mixing efficiency of 98.02% in a short length of 1858 microns. Cheri *et al.* (2013) proposed eight planar micromixer designs using four different shapes of obstacles (Straight (S), Arc (A), Chevron (Ch), and Check Mark (CM)) in two different chambers (round corner rectangular (RCR) and hexagon (H)). Using numerical simulations for the mixing analysis in the Reynolds number range of 0.1–40, it was found that the RCR-S mixer showed optimum performance among the eight mixers with a maximum value of mixing efficiency to pressure drop ratio. The experimental data verified the numerical results that RCR-S micromixer achieved a mixing efficiency of 0.89 and 0.99 in a length of 1.18 *mm* at $Re = 0.1$ and 40, respectively. The RCR and H chambers with different obstacles showed minimum pressure drop and maximum efficiency, respectively.

The sinusoidal form of sub-channels, which inherently have contraction and expansion passages, exhibited significant mixing improvement. The divergence angle plays a critical role in a diverging mixing chamber. Further, a round-cornered rectangular mixing chamber is preferred over a sharp-cornered rectangle. The baffles in a mixing chamber increase fluid chaos leading to higher mixing.

2.3 Lamination-based designs

The lamination-based passive micromixers implement parallel (SadAbadi *et al.*, 2013) and sequential/serial (Lim *et al.*, 2011) lamination techniques to enhance mixing performance. In parallel lamination, each mixing fluid stream is divided into two or more streams which are joined together to form a single stream comprising alternate layers of each mixing fluid side by side. While in sequential/serial lamination mixer designs, the fluid stream (from the inlet) is split and recombined serially (Taheri *et al.*, 2019). Here two or more sub-streams emerge from the inlet stream, and at the recombining point, they are joined again as a single stream. As the number of sub-streams increases, the mixing performances are enhanced. Lim *et al.* (2011) compared the mixing performance of a 3D (CMM) with a conventional passive micromixer applying numerical simulations and experiments (Lim *et al.* 2011). They modified CMM by adding six layers of horizontally and vertically crossing manifold micromixer (H/V-CMM) and achieved a mixing efficiency of over 90% in a channel of length (250 mm) less than five times the channel width. The split-and-recombine and the momentum of the fluids were the main mixing mechanisms in theses designs. Moreover, in a lamination based passive micromixers, there can be crossing manifold structure with horizontally crossing manifold micromixer (H-CMM), and vertically crossing manifold micromixer (V-CMM).

Buchegger *et al.* (2011) proposed a horizontal multi-lamination micromixer having wedge-shaped vertical fluid inlets for enhanced mixing performance in a short time. The wedge-shaped inlets produced uniform lamination layers, which were not observed in the micromixer with a straight inlet. Nakahara *et al.* (2011) proposed a 3D passive lamination micromixer comprised of a multilayered flow generator. By using the proposed technique of the flow generator, multilayer flows were combined in a channel to generate fluid layers with reduced diffusion length. The experimental Investigation showed that the proposed design achieved 1.64 times faster mixing compared to a micromixer with Y-inlet.

Generally, the mixing increases with the increase in the number of sub-streams. The wedge-shaped inlets produce uniform diffusion layers hence, improved mixing efficiency. Further, crossing manifolds, although they increased the width of the mixing channel, improved the mixing efficiency significantly.

2.4. Based on flow obstacles

The obstacles in the flow streams enhance the mixing performance through the generation of vortices and

chaotic advection, thereby shortening the diffusion path length. Depending upon the positioning of the obstacles, the passive micromixers can be categorized as micromixers with obstacles furrowed/attached to the sidewalls, micromixers with obstacles inside the channels, i.e., attached to the top/bottom wall, and micromixers with herringbone grooves/ribs as obstacles.

2.4.1. Obstacles furrowed/attached/embedded on the channel sidewalls

Under this category, the designs with obstacles of different shapes attached to the sidewalls of the straight/curved microchannels are discussed. Nason *et al.* (2014) numerically studied flow and mixing in a 3D channel with rectangular- and triangular-shaped obstacles on the walls for Reynolds numbers in the range of 10 to 100.

The effect of phase shift of obstacles, channel aspect ratio, and obstacle height on mixing and pressure drop were studied. The greater phase shift of the obstacles produced enhanced mixing because of increased recirculation in the cross-section along with a lower pressure drop compared to a no-phase shift of the obstacles. The design having triangular-shaped obstacles achieved higher mixing performance and lower pressure drop than the design with rectangular-shaped obstacles. The effect of the channel aspect ratio on the mixing was insignificant, but the pressure drop varied significantly and showed the highest pressure drop for the highest aspect ratio. Furthermore, the design with the largest obstruction height showed maximum mixing at higher Reynolds numbers.

Sarma and Patowari (2016) numerically investigated the mixing and pressure drop in passive micromixers with rectangular-, triangular- and semicircular-shaped obstructions attached to the wall in a flow of ultra-low Reynolds number of 0.053334. The authors investigated the effects of different parameters, i.e., intersection angle between the inlets (E_θ), obstacle arrangement, obstacle depth, channel aspect ratio (AR), and obstacle packing factor (OPF) on mixing efficiency, and found that the design with rectangular-shaped obstacles achieved the highest mixing with the highest pressure drop, while triangular and semi-circular obstacles had a similar mixing performance. The design with triangular obstacles showed the least pressure drop among these designs. The design with a staggered arrangement showed the highest mixing without significant change in pressure drop. Moreover, the greater obstacle depth and obstacle packing factor increased both mixing and pressure drop, whereas a larger entrance angle enhanced mixing with a negligible effect on the pressure drop.

Wang *et al.* (2015) investigated numerically mixing in a channel with symmetrical cylindrical furrows /grooves for Re = 1–500. They reported that the addition of grooves in the channel increased the mixing performance by 2.22 and 2.18 times compared to conventional Y-micromixer at Re = 10 and 100, respectively. Vijayanandh *et al.* (2019) studied the effect of different shapes (square, curved, and triangular) of ridges attached to the wall of a meandering channel. They reported that the channel with triangular-shaped ridges has higher mixing performance compared to the geometries with square- and curved-shaped ridges.

Tsai and Wu (2011) designed a planar passive micromixer consisting of radial baffles in a curved channel. Multidirectional vortices, i.e., Dean Vortices due to the curved channel and longitudinal vortices due to the radial obstacles, produced significant mixing in this design. Milotin and Lelea (2016) investigated mixing in three passive micromixers (design with no baffle in microtube, design with four baffles covering the half of the cross-section, and the design with four baffles covering the quarter of the cross-section) for Re = 0.2 – 91. The baffles covering the quarter of the cross-section showed higher mixing for all Re values due to rotational flow, increased interface area and higher residence time caused by 90°– delayed orifice.

Lin *et al.* (2011) designed a chaotic micromixer consisting of a square-wave structure and periodic cubic grooves. The experimental comparison indicated that the overall performance was better than the performances of Accoris, slit interdigital, caterpillar, and T-mixer for Re values from 30 to 220. The higher mixing was due to the combined effect of flow stretching (caused by cubic grooves) and laminar recirculation (caused by square-wave structure).

Fractal structures such as Cantor, Minkowski, and Koch have also been used as obstacles by many researchers to enhance mixing. Wu and Chen (2019b) proposed a rectangular fractal-based micromixer named imitate Cantor structure (ICS). The effects of fractal obstacle number, obstacle height, fractal series, and obstacle spacing on mixing were studied using numerical simulations. The better performance of a quadratic fractal series with four obstacles as compared to the primary fractal series with the same number of obstacles indicated that the increase in the number of obstacles and fractal series has a positive impact on the mixing. Furthermore, a staggered arrangement with zero spacing and the largest height showed efficient performance due to vortex generation.

Wu and Chen (2019a) introduced a 3D micromixer consisting of a Cantor structure termed as Imitate Cantor Structure Micromixer (ICSM). The Cantor-based obstacle improved mixing with the mechanisms of chaotic advection and folding of fluid interfaces. They investigated the impact of channel height, obstacle height, the spacing between the obstacles, and fractal obstacles arrangement on mixing performance for Reynolds numbers ranging from 0.01 to 100. Different configurations were obtained through variations in the above-mentioned parameters, which showed mixing performance of over 90% for 0.1 > Re > 50. The ICSM with a channel height of 600 μm showed the best performance with a minimum efficiency of 85% over the entire range of Re. The

increase in the channel height increased an increase in the effective area for fluid folding and, thus, mixing.

Chen and Chen (2020) examined the effect of Minkowski fractal obstacles of both primary and secondary types on the mixing and pressure drop at *Re* = 0.01, 0.1, 1, 10, and 100. The micromixer with secondary Minkowski fractal obstacles showed better mixing than the micromixer with primary type obstacles with a value of more than 98% at *Re* = 0.01, 0.1, and 100, but with a higher pressure drop. Mixing was enhanced due to vortex formation and chaotic convection with an increase in the obstacle height and a reduction in the obstacle spacing. The vortex due to fractal obstruction was more obvious in the micromixer with minimum obstacle spacing, maximum obstacle height, and the highest Reynolds number.

Zhang and Chen (2018) examined the impact of height, spacing, numbers, and configurations of the Koch fractal obstacles attached to the sidewalls on mixing performance. They concluded that greater height, more number, and less spacing of the obstacles have a positive effect on mixing performance. Different configurations formed with four obstacles have a negligible effect on the mixing. The vortex areas produced due to the obstacle helped the mixer to achieve an efficiency of more than 90% at *Re* = 0.03 and 240. In a similar study with Koch fractal obstacle, X.

Chen and Tian (2020) studied the effects of depth, spacing, number, angular inclination, and distribution of baffles on the mixing. The configuration with the bilateral arrangement showed better mixing than the single-sided baffle structure at $Re \geq 10$. Furthermore, the design with a lesser spacing, more numbers, and higher inclination of baffles showed better mixing performance. Chen *et al.* (2019b) studied the effects of rounding the corners of obstacles and examined mixing in the primary fractal micromixer (PFM), secondary fractal micromixer (SFM), and rounding the corners of the secondary fractal micromixer (RCSM). They noticed a higher mixing efficiency of SFM (over 90 % at 0.1, 1, 10, and 100) and RCSM compared to PFM. The rounding of the corner reduced the pressure drop significantly with a slight decrease in mixing compared to SFM.

Chen and Chen (2019) proposed several topological micromixers with circular structures (TMCs) with different ratios of an obstacle to channel height using the topological optimization method. The obstacles reversed the flow and promoted mixing through an increased flow path at low-*Re* and enhanced chaotic advection at high-*Re*. The mixing was obtained in the configuration $TMC_{0.75}$ with an efficiency of more than 90% over the entire *Re*-range. The chaotic advection in the circular mixer was seen at *Re* = 50, while in the TMC mixer, it was observed at *Re* = 10. Cortes-Quiroz *et al.* (2010) performed numerical Simulation and Optimization of a T- micromixer having curved baffles attached to the wall over a Reynolds number range of 1–250. They studied the effects of baffle radius, baffle pitch, and height of the channel on the mixing and pressure drop. The mixing was enhanced due to recirculation and transversal flows caused by the radial baffles. Besides, the curved shape reduces dead volumes and the issue of clogging in the mixer. The proposed design achieved a mixing of over 85% for *Re* = 1 and ≥ 50. However, due to the larger pressure drop for *Re* > 100, a Reynolds number range of 50–100 was recommended for efficient operation.

Xu and Chen (2019) proposed four passive micromixers, i.e., common micromixer (CM), common micromixer with scaling elements (CMWSE), snake-like micromixer (SM), and snake-like micromixer with scaling elements (SMWSE), and evaluated their mixing performance and pressure drop using numerical simulations. They observed that scaling elements enhance chaotic advection and thus positively affect the mixing performance. The order of mixing performance exhibited was as SMWSE (over 92 %) > SM > SMWSE > CM. However, the pressure drop in the mixers with scaling elements was found to be higher than in the designs without it.

The recirculation and transverse flow induced by the baffle, obstacles, and groves on the channel walls, in general, increased flow mixing, which is further increased with the increase in the height of the obstacles/baffles. Further, the packing factor and spread of these obstacles significantly affect the mixing and pressure drop in the channel. The secondary fractals add to the mixing phenomena; moreover, rounding of fractal corners reduces pressure drop significantly with a small decrease in mixing performance.

2.4.2. Obstacles attached to the top/bottom walls

Several researchers have performed the mixing enhancement by placing obstacles inside the channel by attaching them to the top/bottom walls.

Monaco et al. (2010) studied the effects of different shapes and arrangements of obstacles on the mixing in a T-mixer using the Lattice-Boltzmann method. They reported that the layout of obstacles is a more dominant factor for mixing enhancement than using many obstacles. Furthermore, rectangular-shaped obstacles showed the best mixing. Chen and Zhao (2017) performed the Optimization of obstacles-layout in a T-mixer through an orthogonal experiment and investigated the decreasing order of sensitive parameters, i.e., obstacles height > geometric shape > symmetric layout = a number of obstacles. The optimized multi-unit obstacle micromixer showed more than 90% mixing over a wide range of Peclet numbers. The blockage due to the obstacles changed the velocity field and promoted chaotic advection to enhance the mixing.

Alam *et al.* (2014) studied the impact of cylindrical obstacles in a curved microchannel on the mixing performance, applying numerical simulations for *Re* values in the range of 0.1 to 60. They noticed higher

mixing efficiency for the design with cylindrical obstacles in a curved microchannel (88 % at *Re* =0.1 and *Re* > 15) compared to the designs with circular obstacles in a T-shape channel and a simple curved channel. The circular and hexagonal obstructions showed similar mixing performances at all *Re* values; on the other hand, diamond obstructions had less mixing performance except at *Re* = 50. Wang et al. (2014) proposed a passive mixer with triangular baffles embedded in the main channel and evaluated mixing both experimentally and numerically at different *Re* values ranging from 0.1 to 500. The proposed design showed higher mixing (2.48, 4.75, and 8.32 times at *Re* = 1.0, 100, and 500, respectively) than a conventional Y-shape mixer. The mixing increased with the increase in the apical angles of the triangle and the number of triangles.

Out of cross, triangle, pentagon, star, hexagon, and I-shape obstacles in the Y-shape passive micromixers, obstacles with sharp edges showed higher mixing performance. The mixing performance of cross, star-, and I-shaped obstacles was 77%, 75%, and 72%, respectively (Pravinraj and Patrikar, 2019). The addition of a screw-shaped propeller blade in a Y-mixer generated additional flow disturbances in the z-direction and, thus, more mixing compared to a flat-shaped blade (Liu *et al.*, 2014). The design, even with a single screw-shaped propeller blade, achieved a mixing of over 80% for a flow rate of 12 $\mu l/min$. The introduction of a porous twisted tape (permeability = 10^{-10} m^2) in a T-channel improved the mixing at low to medium *Re*, while the solid twisted tape improved the mixing at high-Re (Kurnia and Sasmito, 2019). The twisted tape increased the secondary flow and convective mass transfer with an additional pressure drop. Pendharkar and Patrikar (2014) designed a hexagonal passive micromixer and studied the effects of microchannel fabrication on mixing performance for *Re* values in the range of 0.1 to 0.5. The addition of roughness to the passive mixer geometry resulted in an improvement in mixing (up to 10% at *Re* = 0.1 to 0.5).

Shi *et al.* (2019) numerically studied mixing in a Koch fractal-based obstructions micromixer and reported that the obstruction pattern present on the top wall (same side) of the channel wall produced more mixing (approx. 98.2%, at *Re* = 0.1). Cook *et al.* (2012) designed a planar scaled-up micromixer consisting of an uneven interdigital inlet, staggered teardrop-shaped obstructions, and wall protrusions. The experimental Investigation at *Re* = 1-100 showed that the proposed design achieved the maximum efficiency of 68.5% at *Re* = 1 because of multi-lamination caused by the uneven interdigital inlet. The vortices formed due to the obstructions caused mixing at high Reynolds numbers. The layout of the obstacles is a more significant parameter than the number of obstacles, although mixing efficiency increases with an increase in the number of obstacles, which directly contributes to pressure drop in the channel. The sharp-edged obstacles are more effective for mixing enhancement. Furthermore, the packing of obstacles may have deteriorating effects due to the trapping of fluid on the mixing performance.

2.4.3. Ribs and grooves as obstacles

Many researchers have implemented obstacles in the form of ribs and grooves to enhance the chaotic motion of the fluids and mixing. Several findings have revealed that the more the number of internal ribs, the higher the mixing performance of passive micromixers. The height of a channel affects the flow, and the most effective ratio of the height of the main channel to the herringbone structure was found to be 2:1 (Whulanza *et al.*, 2018). The closely spaced blocks in the microchannel can result in the trapping of fluid and can affect the mixing throughput. Kim *et al.* (2011) studied the effects of four geometric parameters of ribs, such as rib angle, rib height, rib width, and rib spacing numerically, to optimize the mixing performance using the response surface method. The increase in the rib height reduced the area between the wall and rib, which caused the transversal velocity of the vortices to increase and, thus, the mixing. They observed maximum mixing efficiency (over 90 % with channel length 1344 μm) when rib angle, rib height/channel depth, rib width/rib height, and rib spacing/rib height were 35.6°, 0.7, 0.127, and 1.10, respectively. Du *et al.* (2010) analyzed the mixing performances of slanted groove micromixers (SGMs) numerically and staggered herringbone micromixers (SHMs) (Pendharkar, 2014). Single helical flow in SGM and two helical flows, *i.e.*, large vortex for long arm and small vortex for shorter arm in SHM, were observed. Furthermore, a large peak-to-peak distance in the concentration profile and slow convergence were observed in SGM. Hence, faster and more efficient mixing in SHM, while slower and coarser mixing in SGM was noticed.

Guo *et al.* (2010) studied numerically the impact of rib width, pitch, and channel aspect ratio on mixing performance. The mixing performance of the proposed design decreased with the increase of H/W (channel height/channel width) up to a value of 0.6, and beyond that, the influence was negligible. The ribs caused enlargement of the interfacial area, and thus higher mixing was seen with the addition of more ribs and larger width of rib.

In an experiment conducted on a passive scaled-up micromixer with four meandering elements and 36 slanted grooved structures (horizontally stacked), Cook and Hasan (2011) reported higher performance with the increment in the value of *Re* from 5 to 100 due to the formation of Dean vortices. Additionally, Cook *et al.* (2013) designed a scaled-up passive micromixer consisting of a main mixing channel of 155.8 *mm* long, 3 *mm* wide, and 0.75 *mm* deep, with nine slanted grooves, and measured the mixing performance experimentally and numerically for *Re* values ranging from 0.5 to 100. They reported mixing performance

from 53% at *Re* = 5 up to 90% at *Re* = 100. The Dean vortices and helical flows were formed due to the curved channel structure and grooves, respectively. Chen *et al.* (2015) designed a passive micromixer having dual opposing strips on the top and bottom walls of a microchannel and varying cross-sectional area to enhance mixing performance by increasing contact surface area, two-layer vortices generation, and enhanced diffusion flux. The numerical Simulation revealed mixing performance of 93.97%, 92.53%, and 92.49% at *Re* = 0.56, 2.8, and 5.6, respectively. However, misalignment between the top and bottom grooves reduced the mixing.

Fan and Hassan (2010) proposed a curved micromixer with grooves (CMG) and compared its mixing performance with a slanted grooved micromixer (SGM) and curved micromixer without grooves (CM) for Re values in the range of 1 to 50. CMG showed better performance than SGM and CM. In addition, both CMG and SGM achieved better mixing than CM at *Re* = 1.0. The new design showed 60% mixing efficiency at *Re* = 50 with a 1.8 *kPa* pressure drop. At high *Re* values, the curved channel created the Dean vortices, while slanted grooves generated helical flow at low-*Re* values. The elements optimized for the new design included the slanted angle (θ), the width of the grooves angle (ω), and the height ratio of grooves to channel height (Hg/H).

Okuducu and Aral (2019b) proposed a passive micromixer with semi-circular ridges in the microchannel. The new design with the convex alignment of semi-circular elements was found to have a mixing index and mixing performance more than the classical T-shape mixer by the factors of 8.7 (at *Re* = 1 to 10) and 3.3 (at *Re* = 20), respectively. They reported the enhanced mixing (over 80 %) due to the helicoidal-shaped fluid stream generated by the convex alignment of semi-circular elements for *Re* values from 0.1 and 40. The staggered herringbone design has V-shaped ridges attached to the channel walls, and these arrangements enhance mixing at low *Re* values by creating transverse flow patterns.

Hama *et al.* (2018) proposed a micromixer (reverse-staggered herringbone) based on staggered herringbone design geometry and evaluated the mixing performance both numerically and experimentally. They found that the flow rate ratio of fluids positively affects the mixing; however, the *Re* values impact was not significant in the first three and six cycles.

The number of ribs creates more chaos. Hence more mixing of fluid in the channel, the rib height to channel height ratio is a critical parameter in micromixer design; the larger the ratio greater the mixing. A staggered herringbone groove micromixer, which induces dual helical flows, performs better than a mixer with inline helical grooves.

3. ANALYSIS AND DISCUSSION

The Reynolds number and Peclet number are the two significant parameters for the design of passive micromixers. Hence, for an accurate comparison of the performance of different micromixer designs and configurations, it is essential to define these numbers in a similar manner and at the same location. However, after a thorough literature review, it was noticed that most of the studies had defined these numbers either at the inlets or at the main channel. Therefore, carrying out performance comparisons between different designs based on these numbers is highly cumbersome. Furthermore, the review of studies reveals that most of the studies performed have reported only mixing index without attributing proper significance to the pressure drop encountered, device fabrication methods, design complexity, wettability effects, and surface roughness. Hence, for proper advancement of the micromixer designs and their adoption to real applications, the issues mentioned above should be addressed through a proper design criterion prepared by the research community for future studies. The research studies on micromixers have highlighted that many variables, such as geometric parameters, mixing-channel designs, and flow Reynolds numbers, affect the mixing performance. The high Reynolds number value reduces the contact time between the two fluids and decreases mass diffusion leading to lower efficiency in diffusive mixing-based designs. The fluid mixing at a very low Re value is dominated by the residence time and the total path of the flow (Nason *et al.*, 2014).

This study presents a classification of micromixers into several categories, such as designed inlets, designed mixing channels, lamination phenomenon, and flow obstacles. Additionally, charts and graphs present the study outcomes. Analysis of the research studies has shown important outcomes, which will assist in understanding various aspects of micromixers. Figure 5 shows the published articles and evaluation methods used in the studies. The year 2019 reported the highest number of studies, followed by 2014, 2015, 2011, and 2018. The performance evaluation methods used in these studies are mainly numerical simulations or both numerical simulations and experiments, while very few have carried out the only experimental study. The maximum number of studies correspond to experiments and numerical simulations together, followed by numerical simulations alone. Most of the studies revealed that numerical simulations show relatively higher mixing than the actual value achieved through experiments. But a great deal of work has been done on mixing performance via numerical simulations. However, the reliability of the results is always doubtful due to external factors of the real environment unless they are substantiated with experiments. Hence, there is a need to conduct more studies with experiments for measuring the micromixer performance rather than doing only numerical simulations.

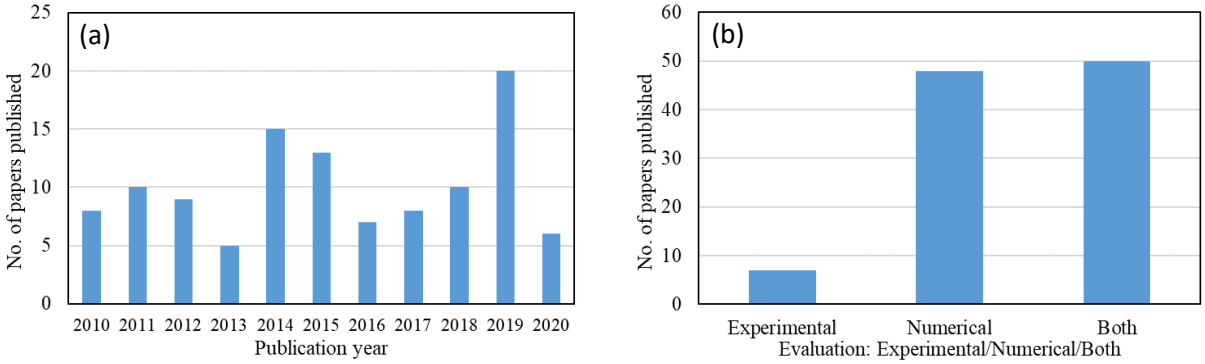

Figure 5. (a) The number of published articles on passive micromixers, and (b) Evaluation methods used in passive micromixers.

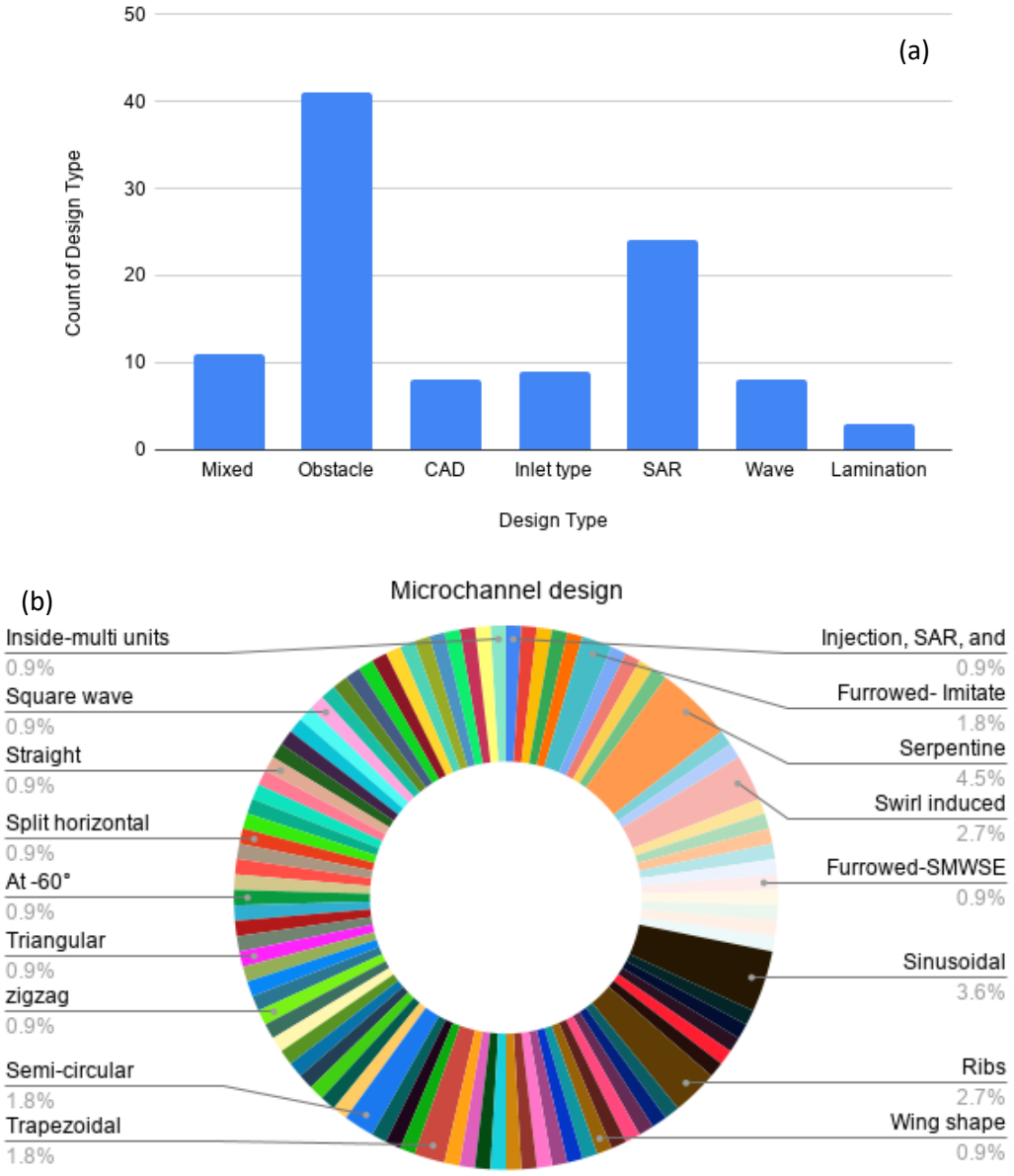

Figure 6. (a) Design type as reported in different studies, and (b) Mixing-channel designs as reported in different studies.

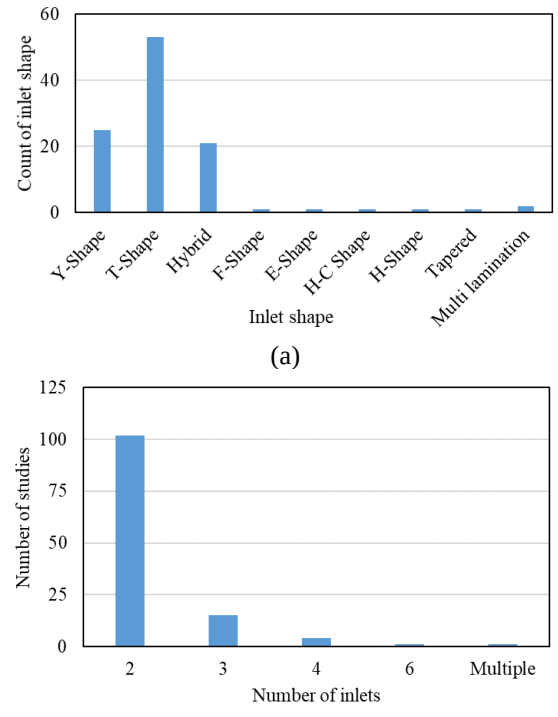

Figure 7. (a) Number of articles with different inlet shape, and (b) Number of inlets as reported in the existing studies.

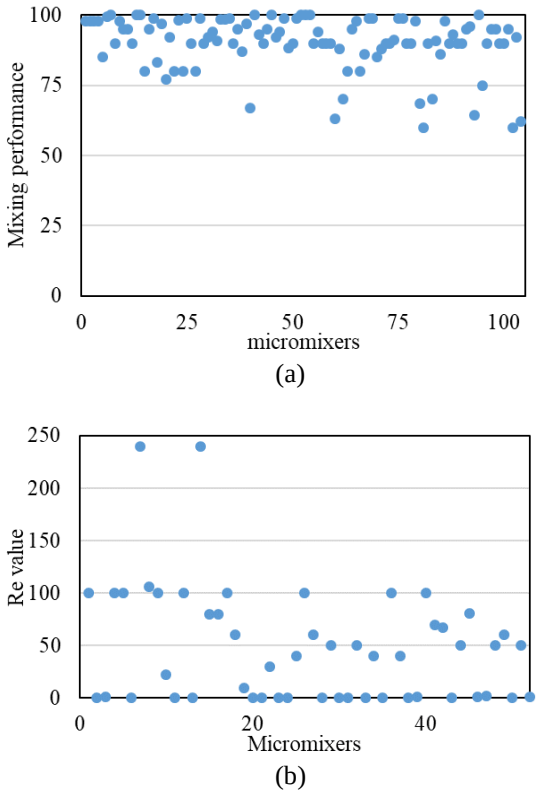

Figure 8. (a) The mixing performance of passive micromixers, and (b) *Re* values considered in the existing studies.

Figure 6 shows the distribution of the studies carried out under different microchannel categories and mixing-channel designs. It shows that the maximum number of obstacle-based designs have been proposed, followed by SAR, mixed category, designed inlet, C-D, and wave. The microchannel has various designs as sinusoidal, square, trapezoidal, etc.

The passive micromixers have inlet shapes as Y-, T-, F-, E-, H-C, Tapered, and hybrid. The number of studies on micromixers is plotted against inlet shape. The maximum number of passive micromixers reported have inlet shape as T-, followed by Y-, and hybrid. Moreover, the most reported number of inlets is two, followed by three. Most of the researchers who reported high performance have used two inlets. Figure 7 shows the distribution of studies reported under different inlet shapes and their numbers.

Most of the studies have reported achieving maximum mixing performance between 80 and 100%. Very few of them have shown mixing performance between 60 to 75 %. Figure 8 shows the mixing performance of passive micromixers and the range of *Re* values reported in the existing studies.

Although the results of the analysis cannot firmly establish the superiority of one method over the others, it can qualify for demonstrating the trends of passive micromixer performance concerning different factors. Appendix A presents the reported studies with above 90% mixing performance, including *Re* values, designs, and other details.

4. CONCLUSION

The number of articles on passive micromixers has increased significantly due to proposed wider applications; however, the research on the mixing performance and micromixer designs is highly fragmented. This review of designs and mixing performance of micromixers have classified passive micromixers based on the designed inlets, mixing-channel design, fluid lamination, and obstacles in the channel. Based on this review study, the following points can be concluded:

1. Most of the researchers have used numerical simulations for evaluating micromixer designs, although the simulation results are not always comparable to physical experiments.
2. Micromixers with T-shape inlets and two inlets are the most preferred choice of micromixers researchers. The obstacles and SAR-based micromixer designs have the edge over other types. Moreover, new mixing-channel designs, such as the Koch fractal and Minkowski fractal, are under Investigation for higher mixing performance.
3. Although several designs have demonstrated higher mixing performance using water-dye experimental and numerical studies, there is a scarcity of work that can demonstrate their capabilities in real applications. Furthermore, in most of these works, little consideration has been

given to the required device material and fabrication process.

4. The open literature lacks micromixer classification based on microfluidic applications.
5. The adoption of micromixers to the real application is highly dependent upon the ease of fabrication and device integration. Hence, future research should consider the factors like material, fabrication method, and design integration along with capabilities in proposed applications.
6. The micromixer designs demonstrating good merit in these aspects, in addition to better mixing, will help integrate them into microsystems for actual applications and accelerate the market growth of microfluidic systems.

CONFLICT OF INTEREST

The authors have no conflict of interest.

FUNDING

Deanship of Research Fund, Grant No. RF/ENG/MEID/19/01.

ACKNOWLEDGMENT

The authors acknowledge the support of Sultan Qaboos University, Oman, for conducting this research.

REFERENCES

Adam T, Hashim U (2012), Simulation of passive fluid driven micromixer for fast reaction assays in nano lab-on-chip domain. Procedia engineering(50): 416-425.

Afzal A, Kim K-Y (2012), Passive split and recombination micromixer with convergent–divergent walls. Chemical Engineering Journal 203: 182-192.

Afzal A, Kim K-Y (2015a), Convergent–divergent micromixer coupled with pulsatile flow. Sensors and Actuators B: Chemical 211: 198-205.

Afzal A, Kim K-Y (2015b), Multi-objective Optimization of a passive micromixer based on periodic variation of velocity profile. Chemical engineering communications 202(3): 322-331.

Al-Halhouli Aa, Alshare A, Mohsen M, Matar M, Dietzel A, Büttgenbach S (2015), Passive micromixers with interlocking semicircle and omega-shaped modules: Experiments and simulations. Micromachines 6(7): 953-968.

Alam A, Afzal A, Kim K-Y (2014), Mixing performance of a planar micromixer with circular obstructions in a curved microchannel. Chemical Engineering Research and Design 92(3): 423-434.

Ansari MA, Kim K-Y (2010), Mixing performance of unbalanced split and recombine micomixers with circular and rhombic sub-channels. Chemical Engineering Journal 162(2): 760-767.

Ansari MA, Kim K-Y, Anwar K, Kim SM (2010), A novel passive micromixer based on unbalanced splits and collisions of fluid streams. Journal of Micromechanics and Microengineering 20(5): 055007.

Ansari MA, Kim K-Y, Kim SM (2018), Numerical and experimental study on mixing performances of simple and vortex micro T-mixers. Micromachines 9(5): 204.

Bayareh M, Ashani MN, Usefian A (2019), Active and passive micromixers: A comprehensive review. Chemical Engineering and Processing-Process Intensification 147: 107771.

Bazaz SR, Mehrizi AA, Ghorbani S, Vasilescu S, Asadnia M, Warkiani ME (2018), A hybrid micromixer with planar mixing units. RSC Advances 8(58): 33103-33120.

Bhopte S, Sammakia B, Murray B (2010), "Numerical study of a novel passive micromixer design," in Proc. 2010 12th IEEE Intersociety Conference on Thermal and Thermomechanical Phenomena in Electronic Systems, Las Vegas, NV, USA, pp. 1-10.

Buchegger W, Wagner C, Lendl B, Kraft M, Vellekoop MJ (2011), A highly uniform lamination micromixer with wedge shaped inlet channels for time resolved infrared spectroscopy. Microfluidics and Nanofluidics 10(4): 889-897.

Chen P-C, Pan C-W, Kuo Y-L (2015), Performance characterization of passive micromixer with dual opposing strips on microchannel walls. Chemical Engineering and Processing: Process Intensification 93: 27-33.

Chen X, Li T (2017), A novel passive micromixer designed by applying an optimization algorithm to the zigzag microchannel. Chemical Engineering Journal 313: 1406-1414.

Chen X, Li T, Li X (2016a), Numerical research on shape optimization of microchannels of passive micromixers. IEEE Sensors Journal 16(17): 6527-6532.

Chen X, Li T, Zeng H, Hu Z, Fu B (2016b), Numerical and experimental Investigation on micromixers with serpentine microchannels. International Journal of Heat and Mass Transfer 98: 131-140.

Chen X, Liu S, Chen Y, Wang S (2019a), A review on species mixing in droplets using passive and active micromixers. International Journal of Environmental Analytical Chemistry 101:422-432.

Chen X, Shen J, Hu Z (2018), fabrication and performance evaluation of two multilayer passive micromixers. Sensor Review 38(3): 321-325.

Chen X, Tian Y (2020), Passive micromixer with baffles distributed on both sides of microchannels based on the Koch fractal principle. Journal of Chemical Technology & Biotechnology 95(3): 806-812.

Chen X, Zhang S, Wu Z, Zheng Y (2019b), A novel

Koch fractal micromixer with rounding corners structure. Microsystem Technologies 25(7): 2751-2758.

Chen X, Zhao Z (2017), Numerical Investigation on layout optimization of obstacles in a three-dimensional passive micromixer. Analytica chimica acta 964: 142-149.

Chen Y, Chen X (2019), An improved design for passive micromixer based on topology optimization method. Chemical Physics Letters 734: 136706.

Chen Y, Chen X (2020), Numerical Investigations of a Passive Micromixer Based on Minkowski Fractal Principle. International Journal of Chemical Reactor Engineering 18(2): 20190105.

Cheri MS, Latifi H, Moghaddam MS, Shahraki H (2013), Simulation and experimental Investigation of planar micromixers with short-mixing-length. Chemical Engineering Journal 234: 247-255.

Chung C-K, Shih T, Wu B, Chang C (2010), Design and mixing efficiency of rhombic micromixer with flat angles. Microsystem Technologies 16(8-9): 1595-1600.

Cook K, Fan Y, Hassan I (2011), "Experimental Investigation of a Scaled-Up Passive Interdigital Micromixer With Circular-Sector Mixing Elements," in Proc. ASME/JSME 2011 8th Thermal Engineering Joint Conference, Honolulu, Hawaii, USA, pp. T10118

Cook KJ, Fan Y, Hassan I (2012), Experimental Investigation of a scaled-up passive micromixer with uneven interdigital inlet and teardrop obstruction elements. Experiments in fluids 52(5): 1261-1275.

Cook KJ, Fan Y, Hassan I (2013), Mixing evaluation of a passive scaled-up serpentine micromixer with slanted grooves. Journal of fluids engineering 135(8).

Cook KJ, Hassan IG (2011), "Experimental Investigation of a Scaled-Up Passive Curved Channel Micromixer With Slanted Grooves," in Proc. ASME 2011 9th International Conference on Nanochannels, Microchannels, and Minichannels, Edmonton, Alberta, Canada, pp. 111-117.

Cortes-Quiroz CA, Azarbadegan A, Moeendarbary E, Zangeneh M (2010), "Analysis and optimization of a passive micromixer with curved-shaped baffles for efficient mixing with low pressure loss in continuous flow," in Proc. ASME 2010 8th International Conference on Nanochannels, Microchannels, and Minichannels collocated with 3rd Joint US-European Fluids Engineering Summer Meeting, Montreal, Canada, pp. 1347-1355.

Du Y, Zhang Z, Yim C, Lin M, Cao X (2010), Evaluation of floor-grooved micromixers using concentration-channel length profiles. Micromachines 1(1): 19-33.

Dundi TM, Raju V, Chandramohan V (2019), Numerical evaluation of swirl effect on liquid mixing in a passive T-micromixer. Australian Journal of Mechanical Engineering: 1-15.

Fan Y, Hassan I (2010a), Experimental and numerical Investigation of a scaled-up passive micromixer using fluorescence technique. Experiments in fluids 49(3): 733-747.

Fan Y, Hassan I (2010b), "Numerical Simulation of a Novel Passive Micromixer With Curved Channel and Slanted Grooves," in Proc. ASME 2010 8th International Conference on Nanochannels, Microchannels, and Minichannels collocated with 3rd Joint US-European Fluids Engineering Summer Meeting, Montreal, Canada, pp. 1203-1212.

Gaozhe C, Li X, Huilin Z, Jianhan L (2017), A Review on Micromixers. Micromachines 8(274): 27.

Gidde RR, Pawar PM (2020), Flow feature and mixing performance analysis of RB-TSAR and EB-TSAR micromixers. Microsystem Technologies 26(2): 517-530.

Gidde RR, Pawar PM, Gavali SR, Salunkhe SY (2019a), Flow feature analysis of an eye shaped split and collision (ES-SAC) element based micromixer for lab-on-a-chip application. Microsystem Technologies 25(8): 2963-2973.

Gidde RR, Pawar PM, Ronge BP, Misal ND, Kapurkar RB, Parkhe AK (2018), Evaluation of the mixing performance in a planar passive micromixer with circular and square mixing chambers. Microsystem Technologies 24(6): 2599-2610.

Gidde RR, Pawar PM, Ronge BP, Shinde AB, Misal ND, Wangikar SS (2019b), Flow field analysis of a passive wavy micromixer with CSAR and ESAR elements. Microsystem Technologies 25(3): 1017-1030.

Guo L, Zhang S, Han K (2010), "Numerical Simulation of Mixing Performances of a Passive Micromixer with Internal Ribs," in Proc. AIP Conference Proceedings 1207(1), Xi'an, China, pp. 1024-1029.

Hama B, Mahajan G, Fodor PS, Kaufman M, Kothapalli CR (2018), Evolution of mixing in a microfluidic reverse-staggered herringbone micromixer. Microfluidics and Nanofluidics 22(5): 54.

Hong W, Shi H, Huang Z, Long M, Xu H, Liu Z (2019), Design and Simulation of a passive micromixer with gourd-shaped channel. Journal of nanoscience and nanotechnology 19(1): 206-212.

Hossain S, Kim K-Y (2014), Mixing analysis of passive micromixer with unbalanced three-split rhombic sub-channels. Micromachines 5(4): 913-928.

Hossain S, Kim K-Y (2015), Mixing analysis in a three-dimensional serpentine split-and-recombine micromixer. Chemical Engineering Research and Design 100: 95-103.

Hossain S, Lee I, Kim SM, Kim K-Y (2017), A micromixer with two-layer serpentine crossing channels having excellent mixing performance at low Reynolds numbers. Chemical Engineering

Journal 327: 268-277.

Hsieh S-S, Lin J-W, Chen J-H (2013), Mixing efficiency of Y-type micromixers with different angles. International Journal of Heat and Fluid Flow 44: 130-139.

Jang H, Pawate AS, Bhargava R, Kenis PJA (2019), Polymeric microfluidic continuous flow mixer combined with hyperspectral FT-IR imaging for studying rapid biomolecular events. Lab Chip 19(15): 2598-2609.

Jaywant SA, Arif KM (2019), A Comprehensive Review of Microfluidic Water Quality Monitoring Sensors. Sensors (Basel) 19(21).

Jeong GS, Chung S, Kim CB, Lee SH (2010), Applications of micromixing technology. Analyst 135(3): 460-473.

Johnson TJ, Locascio LE (2002), Characterization and Optimization of slanted well designs for microfluidic mixing under electroosmotic flow. Lab on a Chip 2: 135.

Kastania AS, Tsougeni K, Papadakis G, Gizeli E, Kokkoris G, Tserepi A, Gogolides E (2016), Plasma micro-nanotextured polymeric micromixer for DNA purification with high efficiency and dynamic range. Anal Chim Acta 942: 58-67.

Kefala I, Papadopoulos VE, Kokkoris G, Karpou G, Moschou D, Papadakis G, Tserepi A (2014), A Passive Micromixer for Bioanalytical Applications, in Proc 4th Micro and Nano Flows Conference, UCL, London, UK, pp. 1-8.

Khan AA, Tandon U (2017), Simulation of Wing-shaped Passive Micromixers using COMSOL. International Journal of Computer Science Engineering (IJCSE) 6(1): 10-17.

Kim BS, Kwak BS, Shin S, Lee S, Kim KM, Jung H-I, Cho HH (2011), Optimization of microscale vortex generators in a microchannel using advanced response surface method. International Journal of Heat and Mass Transfer 54(1-3): 118-125.

Kurnia JC, Sasmito AP (2019), Performance Evaluation of Liquid Mixing in a T-Junction Passive Micromixer with a Twisted Tape Insert. Industrial & Engineering Chemistry Research 59(9): 3904-3915.

Le The H, Le-Thanh H, Tran-Minh N, Karlsen F (2014), "A novel passive micromixer with trapezoidal blades for high mixing efficiency at low Reynolds number flow," in Proc. 2nd Middle East Conference on Biomedical Engineering, pp. 25-28.

Le The H, Le Thanh H, Dong T, Ta BQ, Tran-Minh N, Karlsen F (2015), An effective passive micromixer with shifted trapezoidal blades using wide Reynolds number range. Chemical Engineering Research and Design 93: 1-11.

Lee C-Y, Fu L-M (2018), Recent advances and applications of micromixers. Sensors and Actuators B: Chemical 259: 677-702.

Li L, Chen QD, Tsai C (2014), Three dimensional triangle chaotic micromixer. Advanced Materials Research 875-877: 1189-1193.

Li X, Chang H, Liu X, Ye F, Yuan W (2015), A 3-D overbridge-shaped micromixer for fast mixing over a wide range of reynolds numbers. Journal of Microelectromechanical Systems 24(5): 1391-1399.

Lim TW, Son Y, Jeong YJ, Yang D-Y, Kong H-J, Lee K-S, Kim D-P (2011), Three-dimensionally crossing manifold micro-mixer for fast mixing in a short channel length. Lab on a Chip 11(1): 100-103.

Lin Y, Yu X, Wang Z, Tu S-T, Wang Z (2011), Design and evaluation of an easily fabricated micromixer with three-dimensional periodic perturbation. Chemical Engineering Journal 171(1): 291-300.

Liu K, Yang Q, Chen F, Zhao Y, Meng X, Shan C, Li Y (2015), Design and analysis of the cross-linked dual helical micromixer for rapid mixing at low Reynolds numbers. Microfluidics and Nanofluidics 19(1): 169-180.

Liu Y-J, Chen P-Y, Yang J-Y, Tsou C, Lee Y-H, Baldeck P, Lin C-L (2014), Three-dimensional passive micromixer fabricated by two-photon polymerization for microfluidic mixing. Sensors and Materials 26(2): 39-44.

Matsunaga T, Nishino K (2014), Swirl-inducing inlet for passive micromixers. RSC Advances 4(2): 824-829.

Mehrdel P, Karimi S, Farré-Lladós J, Casals-Terré J (2018), Novel Variable Radius Spiral–Shaped Micromixer: From Numerical Analysis to Experimental Validation. Micromachines 9(11): 552.

Milotin R, Lelea D (2016), The passive mixing phenomena in microtubes with baffle configuration. Procedia Technology 22: 243-250.

Moghimi M, Jalali N (2020), Design and fabrication of an effective micromixer through passive method. Journal of Computational & Applied Research in Mechanical Engineering (JCARME) 9(2): 371-383.

Monaco E, Luo KH, Brenner G (2010), "Numerical Investigation on the efficiency of a passive micromixer with the lattice Boltzmann method," in Proc. V European Conference on Computational Fluid Dynamics ECCOMAS CFD, Lisbon, Portugal, pp. 1-20.

Mondal B, Mehta SK, Patowari PK, Pati S (2019), Numerical study of mixing in wavy micromixers: comparison between raccoon and serpentine mixer. Chemical Engineering and Processing-Process Intensification 136: 44-61.

Mukhopadhyay S (2018), Short Review on the Classification of Micromixers. International Journal of Composite Materials and Matrices 4(1): 1-3.

Nakahara T, Ootani N, Asanuma T, Hagio Y, Hiramaru D, Terao K, Okonogi A, Oohira F, Kotera H, Suzuki T (2011), "Development of a Three Dimensional Passive Lamination Micromixer," in Proc. ASME-JSME-KSME 2011 Joint Fluids Engineering Conference, Hamamatsu, Japan, pp.

371-373.
Nason F, Pennati G, Dubini G (2014), Computational modeling of passive furrowed channel micromixers for lab-on-a-chip applications. Journal of applied biomaterials & functional materials 12(3): 278-285.
Nimafar M, Viktorov V, Martinelli M (2012), Experimental comparative mixing performance of passive micromixers with H-shaped sub-channels. Chemical engineering science 76: 37-44.
Okuducu MB, Aral MM (2019a), Computational evaluation of mixing performance in 3-D swirl-generating passive micromixers. Processes 7(3): 121.
Okuducu MB, Aral MM (2019b), Novel 3-D T-Shaped Passive Micromixer Design with Helicoidal Flows. Processes 7(9): 637.
Papadopoulos V, Kefala I, Kaprou G, Kokkoris G, Moschou D, Papadakis G, Gizeli E, Tserepi A (2014), A passive micromixer for enzymatic digestion of DNA. Microelectronic Engineering 124: 42-46.
Parsa MK, Hormozi F, Jafari D (2014), Mixing enhancement in a passive micromixer with convergent–divergent sinusoidal microchannels and different ratio of amplitude to wave length. Computers & Fluids 105: 82-90.
Pendharkar G, Deshmukh R, Patrikar R (2014), Investigation of surface roughness effects on fluid flow in passive micromixer. Microsystem Technologies 20(12): 2261-2269.
Pennella F, Rossi M, Ripandelli S, Rasponi M, Mastrangelo F, Deriu MA, Ridolfi L, Kähler CJ, Morbiducci U (2012), Numerical and experimental characterization of a novel modular passive micromixer. Biomedical microdevices 14(5): 849-862.
Pravinraj T, Patrikar R (2019), "Modeling, fabrication and investigation of mixing in low-cost passive PDMS micromixers," in Proc. 2019 32nd International Conference on VLSI Design and 2019 18th International Conference on Embedded Systems (VLSID), Delhi, India, pp. 185-190.
Rafeie M, Welleweerd M, Hassanzadeh-Barforoushi A, Asadnia M, Olthuis W, Ebrahimi Warkiani M (2017), An easily fabricated three-dimensional threaded lemniscate-shaped micromixer for a wide range of flow rates. Biomicrofluidics 11(1): 014108.
Rampalli S, Dundi TM, Chandrasekhar S, Raju V, Chandramohan V (2020), Numerical Evaluation of Liquid Mixing in a Serpentine Square Convergent-divergent Passive Micromixer. Chemical Product and Process Modeling: 11.
Raza W, Hossain S, Kim K-Y (2020), A Review of Passive Micromixers with a Comparative Analysis. Micromachines 11(5): 455.
Ruijin W, Beiqi L, Dongdong S, Zefei Z (2017), Investigation on the splitting-merging passive micromixer based on Baker's transformation. Sensors and Actuators B: Chemical 249: 395-404.
SadAbadi H, Packirisamy M, Wüthrich R (2013), High performance cascaded PDMS micromixer based on split-and-recombination flows for lab-on-a-chip applications. RSC Advances 3(20): 7296-7305.
Sarma P, Patowari PK (2016), Design and analysis of passive Y-type micromixers for enhanced mixing performance for biomedical and microreactor application. Journal of Advanced Manufacturing Systems 15(03): 161-172.
Scherr T, Quitadamo C, Tesvich P, Park DS-W, Tiersch T, Hayes D, Choi J-W, Nandakumar K, Monroe WT (2012), A planar microfluidic mixer based on logarithmic spirals. Journal of Micromechanics and Microengineering 22(5): 055019.
Sheu TS, Chen SJ, Chen JJ (2012), Mixing of a split and recombine micromixer with tapered curved microchannels. Chemical engineering science 71: 321-332.
Shi X, Wang L, Huang S, Li F (2019), A novel passive micromixer with array of Koch fractal obstacles in microchannel. Journal of Dispersion Science and Technology 42(2): 236-247.
Stanciu I (2015), Uncertainty analysis of mixing efficiency variation in passive micromixers due to geometric tolerances. Modelling and Simulation in Engineering 2015: 343087.
Su T, Cheng K, Wang J, Xu Z, Dai W (2019), A fast design method for passive micromixer with angled bend. Microsystem Technologies 25(11): 4391-4397.
Ta BQ, Lê Thanh H, Dong T, Thoi TN, Karlsen F (2015), Geometric effects on mixing performance in a novel passive micromixer with trapezoidal-zigzag channels. Journal of Micromechanics and Microengineering 25(9): 094004.
Taheri RA, Goodarzi V, Allahverdi A (2019), Mixing performance of a cost-effective split-and-recombine 3D micromixer fabricated by xurographic method. Micromachines 10(11): 786.
Tran-Minh N, Dong T, Karlsen F (2014), An efficient passive planar micromixer with ellipse-like micropillars for continuous mixing of human blood. Computer methods and programs in biomedicine 117(1): 20-29.
Tsai R-T, Wu C-Y (2011), An efficient micromixer based on multidirectional vortices due to baffles and channel curvature. Biomicrofluidics 5(1): 014103.
Tseng L-Y, Yang A-S, Lee C-Y, Hsieh C-Y (2011), CFD-based Optimization of a diamond-obstacles inserted micromixer with boundary protrusions. Engineering Applications of Computational Fluid Mechanics 5(2): 210-222.
Vijayanandh V, Pradeep A, Suneesh P, Babu TS (2019), "Design and simulation of passive micromixers with ridges for enhanced efficiency," in Proc. IOP Conference Series: Materials Science and Engineering, Bengaluru, India, pp. 012106.
Viktorov V, Mahmud MR, Visconte C (2015),

Comparative analysis of passive micromixers at a wide range of Reynolds numbers. Micromachines 6(8): 1166-1179.

Viktorov V, Mahmud MR, Visconte C (2016), Design and characterization of a new HC passive micromixer up to Reynolds number 100. Chemical Engineering Research and Design 108: 152-163.

Viktorov V, Nimafar M (2013), A novel generation of 3D SAR-based passive micromixer: efficient mixing and low pressure drop at a low Reynolds number. Journal of Micromechanics and Microengineering 23(5): 055023.

Wang H, Shi L, Zhou T, Xu C, Deng Y (2018), A novel passive micromixer with modified asymmetric lateral wall structures. Asia-Pacific Journal of Chemical Engineering 13(3): e2202.

Wang L, Ma S, Han X (2015), Micromixing enhancement in a novel passive mixer with symmetrical cylindrical grooves. Asia-Pacific Journal of Chemical Engineering 10(2): 201-209.

Wang L, Ma S, Wang X, Bi H, Han X (2014), Mixing enhancement of a passive microfluidic mixer containing triangle baffles. Asia-Pacific Journal of Chemical Engineering 9(6): 877-885.

Westerhausen C, Schnitzler LG, Wendel D, Krzyszton R, Lachelt U, Wagner E, Radler JO, Wixforth A (2016), Controllable Acoustic Mixing of Fluids in Microchannels for the Fabrication of Therapeutic Nanoparticles. Micromachines 7(9): 150.

Whulanza Y, Utomo MS, Hilman A (2018), "Realization of a passive micromixer using herringbone structure," in AIP Conference Proceedings 1933(1), Bali, Indonesia, 040003.

Wu Z, Chen X (2019a), A novel design for 3D passive micromixer based on Cantor fractal structure. Microsystem Technologies 25(1): 225-236.

Wu Z, Chen X (2019b), A novel design for passive micromixer based on Cantor fractal structure. Microsystem Technologies 25(3): 985-996.

Xia G, Li J, Wu H, Zhou M, Wang H (2011), "A Novel Passive Micromixer Based on Asymmetric Split-and-Recombine With Fan-Shaped Cavity," in Proc. ASME 2011 9th International Conference on Nanochannels, Microchannels, and Minichannels, Edmonton, Alberta, Canada, pp. 135-141.

Xie H, Zhao X, Yang H (2010), "Experimental and numerical study on a planar passive micromixer with semicircle mixing elements," in Proc. IEEE/ASME 2010 International Conference on Advanced Intelligent Mechatronics, Montreal, QC, Canada, pp. 1013-1016.

Xu J, Chen X (2019), Numerical study on mixing performance of 3D passive micromixer with scaling elements. Journal of the Brazilian Society of Mechanical Sciences and Engineering 41(10): 453.

Yang A-S, Chuang F-C, Chen C-K, Lee M-H, Chen S-W, Su T-L, Yang Y-C (2015), A high-performance micromixer using three-dimensional Tesla structures for bio-applications. Chemical Engineering Journal 263: 444-451.

Yang J, Qi L, Chen Y, Ma H (2013), Design and fabrication of a three dimensional spiral micromixer. Chinese Journal of Chemistry 31(2): 209-214.

Yang L, Li S, Liu J, Cheng J (2018), Fluid mixing in droplet-based microfluidics with T junction and convergent–divergent sinusoidal microchannels. Electrophoresis 39(3): 512-520.

Zadeh HF, Marahel A (2011), "Simulations of Flow and Mass Transfer in a Passive Micromixer," in Proc. ASME 2011 9th International Conference on Nanochannels, Microchannels, and Minichannels, Edmonton, Alberta, Canada pp. 179-185.

Zhang H, Bai Y, Zhu N, Xu J (2021), Microfluidic reactor with immobilized enzyme-from construction to applications: A review. Chinese Journal of Chemical Engineering 30: 136-145.

Zhang S, Chen X (2018), A novel passive micromixer based on Koch fractal principle. Journal of the Brazilian Society of Mechanical Sciences and Engineering 40(10): 487.

Zhang W, Wang X, Feng X, Yang C, Mao Z-S (2016), Investigation of mixing performance in passive micromixers. Industrial & Engineering Chemistry Research 55(38): 10036-10043.

Zhang Y, Hu Y, Wu H (2012), Design and Simulation of passive micromixers based on capillary. Microfluidics and Nanofluidics 13(5): 809-818.

Appendix A:

Reference	Year	Inlet shape	Inlet no	Design type	Mixing-channel design	Mixing performance (max %)	Re value	Evaluation method
(Moghimi and Jalali, 2020)	2020	Y-Shape	2	Mixed	Injection, SAR, and zigzag	98.02	100	Both Numerical and Experimental
(Chen and Chen, 2020)	2020	T-Shape	2	Obstacle	Furrowed-Secondary Minkowski fractal	98 98 98	0.01 1 100	Numerical Simulation
(Chen and Tian, 2020)	2020	T-Shape	2	Obstacle	Furrowed-Koch fractal (30 angle)	99.48	100	Numerical Simulation
(Rampalli *et al.*, 2020)	2020	T-Shape	2	C-D	Serpentine square	100	160 < Or <180	Numerical Simulation
(Wu and Chen, 2019a)	2019	T-Shape	2	Obstacle	Furrowed-Imitate Cantor structure	90	>=50 Or <=0.1	Numerical Simulation
(Shi *et al.*, 2019)	2019	T-Shape	2	Obstacle	Inside-Koch fractal	98	0.1	Numerical Simulation
(Chen and Chen, 2019)	2019	T-Shape	2	Obstacle	Furrowed-Minkowski fractal	95	>=5	Numerical Simulation
(Chen *et al.*, 2019b)	2019	T-Shape	2	Obstacle	Furrowed-Secondary Koch fractal	95 90	0.05-100 0.1-100	Numerical Simulation
(Mondal *et al.*, 2019)	2019	T-Shape	2	C-D	Raccoon Serpentine	100 100	0.1-100 0.1-100	Numerical Simulation
(Dundi *et al.*, 2019)	2019	T-Shape	2	Designed inlet	Swirl induced	95	106	Numerical Simulation
(Gidde *et al.*, 2019b)	2019	T-Shape	2	SAR	Elliptic	99	20-75	Numerical Simulation
(Xu and Chen, 2019)	2019	Y-Shape	2	Obstacle	Furrowed-SMWSE	92	22	Both Numerical and Experimental
(Shi *et al.*, 2019)	2019	T-Shape	2	Obstacle	Inside-Koch obstacle	98.2	0.1	Numerical Simulation
(Gidde *et al.*, 2018)	2018	T-Shape	2	SAR	Circular and square chamber	99	<1.0	Numerical Simulation
(Zhang and Chen, 2018)	2018	T-Shape	2	Obstacle	Furrowed-Koch fractal	99 90	0.03 240	Numerical Simulation
(Chen *et al.*, 2018)	2018	F-Shape E-Shape	2	SAR	Stacked	92 94	80 80	Both Numerical and Experimental
(Ansari *et al.*, 2018)	2018	T-Shape	2	C-D	Serpentine	91	29221	Both Numerical and Experimental
(Mehrdel *et al.*, 2018)	2018	T-Shape	3	Mixed	Double spiral	98.5	0.1-10	Both Numerical and Experimental

(Hama *et al.*, 2018)	2018	T-Shape	2	Obstacle	Ribs-Reverse staggered herringbone	98.5	100	Both Numerical and Experimental
(Hossain *et al.*, 2017)	2017	Y-Shape	2	SAR	Serpentine	99	0.2-10	Both Numerical and Experimental
(Rafeie *et al.*, 2017)	2017	Y-Shape	2	Wave	Spiral	90	1-1000	Numerical Simulation
(Chen and Li, 2017)	2017	T-Shape	2	Obstacle	Furrowed-Trapezoidal zigzag	95	<=0.5 Or >=5	Both Numerical and Experimental
(Chen *et al.*, 2016a)	2016	T-Shape	2	Obstacle	Furrowed-Trapezoidal zigzag	93	<=0.5 or >=5	Numerical Simulation
(Viktorov *et al.*, 2016)	2016	H-C Shape	2	SAR	H-C	90	>=1 Or <=100	Both Numerical and Experimental
(Chen *et al.*, 2016b)	2016	T-Shape	2	C-D	Serpentine	95	0.1-100	Both Numerical and Experimental
(Milotin and Lelea, 2016)	2016	T-Shape	2	Obstacle	Furrowed-Circular	100	0.2-91	Numerical Simulation
(Afzal and Kim, 2015a)	2015	T-Shape	2	C-D	Sinusoidal	92	0.5	Numerical Simulation
(Chen *et al.*, 2015)	2015	Y-Shape	2	Obstacle	Ribs-Two strips	93.97	0.56	Both Numerical and Experimental
(Le The *et al.*, 2015)	2015	Hybrid	3	SAR	Trapezoidal	90	>= 20, Or <=0.9	Both Numerical and Experimental
(Liu *et al.*, 2015)	2015	Y-Shape	2	Wave	Double helical	99	0.003-30	Both Numerical and Experimental
(Al-Halhouli *et al.*, 2015)	2015	T-Shape	2	Wave	ILSC	100	0.01 - 50	Both Numerical and Experimental
					Omega	100	0.01 - 50	
					Semi-circular	100	> 50	
(Viktorov *et al.*, 2015)	2015	Y-Shape	2	SAR	Chain (Y-Y and H-C)	90	1-100	Both Numerical and Experimental
(Ta *et al.*, 2015)	2015	Hybrid	3	SAR	Trapezoidal zigzag	94	>=20	Both Numerical and Experimental
						90	<=0.9	
(Li *et al.*, 2015)	2015	T-Shape	2	SAR	Overbridge	90	0.01-50	Both Numerical and Experimental
(Yang *et al.*, 2015)	2015	T-Shape	2	SAR	Tesla	90	0.1-100	Both Numerical and Experimental
(Le The *et al.*, 2014)	2014	Hybrid	3	SAR	Trapezoidal	95	40	Both Numerical and

								Experimental
(Parsa *et al.*, 2014)	2014	T-Shape	2	C-D	Sinusoidal	99 99	0.2 >30	Both Numerical and Experimental
(Li *et al.*, 2014)	2014	Y-Shape	2	SAR	Triangular	90	0.01	Numerical Simulation
(Nason *et al.*, 2014)	2014	Y-Shape	2	Obstacle	Furrowed-Triangular	90	50	Numerical Simulation
(Wang *et al.*, 2014)	2014	Y-Shape	2	Obstacle	Inside-Triangular	91.2	0.1	Both Numerical and Experimental
(Cheri *et al.*, 2013)	2013	Hybrid	3	Mixed	Hexagonal chamber	99	40	Both Numerical and Experimental
(Hsieh *et al.*, 2013)	2013	Hybrid	2	Designed inlet	At -60°	99	0.027	Experiment
(Cook *et al.*, 2013)	2013	Y-Shape	2	Obstacle	Ribs	90	100	Both Numerical and Experimental
(Yang *et al.*, 2013)	2013	Y-Shape	2	Wave	Double Spiral	90	40	Both Numerical and Experimental
(Viktorov and Nimafar, 2013)	2013	T-Shape	2	SAR	Chain	98	0.416	Both Numerical and Experimental
(Afzal and Kim, 2012)	2012	T-Shape	2	Mixed	Sinusoidal wall	90	70	Numerical Simulation
(Nimafar *et al.*, 2012)	2012	H-Shape	2	SAR	H-shape	98	0.083	Both Numerical and Experimental
(Sheu *et al.*, 2012)	2012	Tapered	2	SAR	Staggered curve	90	50	Both Numerical and Experimental
(Tsai and Wu, 2011)	2011	Y-Shape	2	Obstacle	Furrowed-Radial	93	81	Both Numerical and Experimental
(Lim *et al.*, 2011)	2011	Multi-lamination	Multiple	Lamination	3D-CMM	90	1	Experiment
(Lin *et al.*, 2011)	2011	Y-Shape	2	Obstacle	Square Wave	90	>=40	Both Numerical and Experimental
(Kim *et al.*, 2011)	2011	T-Shape	2	Obstacle	Rib	95	1.69	Both Numerical and Experimental
(Tseng *et al.*, 2011)	2011	Y-Shape	2	Obstacle	Diamond	96	>10 Or <0.1	Numerical Simulation
(Zadeh and Marahel, 2011)	2011	Hybrid	4	Designed inlet	300°	100	60	Numerical Simulation
(Chung *et al.*, 2010)	2010	Hybrid	3	SAR	Rhombic	95	>180	Both Numerical and Experimental

(Du *et al.*, 2010)	2010	T-Shape	2	Obstacle	Staggered herringbone	95	0.3	Numerical Simulation
(Xie *et al.*, 2010)	2010	T-Shape	2	Mixed	Semi-circular	90	<0.1 Or >10	Both Numerical and Experimental
(Ansari *et al.*, 2010)	2010	T-Shape	2	Mixed	Unbalanced circles	90	>40	Both Numerical and Experimental
(Cortes-Quiroz *et al.*, 2010)	2010	T-Shape	2	Obstacle	Furrowed-Curved	95	50-100	Both Numerical and Experimental
(Bhopte *et al.*, 2010)	2010	Hybrid	4	Designed inlet	Split	92	1	Numerical Simulation